t-J 模型における反強磁性と超伝導

多々良　源

Gen Tatara

Antiferromagnetism and Superconductivity in the t-J model

Gen Tatara
Institute of Physics
University of Tokyo, Komaba

25 December 1991
(Revised 6 February 1992)

Abstract

The antiferromagnetism and superconductivity of the high T_c superconductor are investigated based on the slave fermion representation of the t-J model. The local constraint is taken into account by introducing the CP^1 variable for the spin. Integrating out the spins on one of the sublattice, the effective action of the hole and spin is derived. On this effective theory, the magnetic properties are studied with the effects of holes included systematically. The Néel temperature obtained as a function of doping is in agreement with experiments. Our treatment of the constraint using the CP^1 variable also makes explicit the pairing force between two neighboring holes. The mean field theory of the gauge invariant superconducting order parameter of two holes is performed on the t-J model in this treatment. The ground state is the superconducting flux state. The order parameter has $s+id$ symmetry. The behavior of the critical temperature agrees with experiments qualitatively. The size of the fermi surface obtained in this scheme is, however, small.

Contents

1 Introduction 4

2 Preliminaries 6
- 2.1 High T_c superconductor . . . 6
- 2.2 High T_c material as strongly correlated system . . . 8
- 2.3 t-J model . . . 10
- 2.4 Previous approaches to t-J model . . . 13
- 2.5 Our formalism . . . 16

3 Magnetic properties 17
- 3.1 Derivation of the effective theory . . . 17
- 3.2 Effective CP^1 action . . . 23
- 3.3 Saddle point approximation of the CP^1 model . . . 26
- 3.4 $\alpha \to 0$ limit of the solution at zero doping . . . 30
- 3.5 Numerical solutions at zero doping . . . 33
- 3.6 Solutions at finite doping . . . 36
- 3.7 Short range spiral state . . . 37
- 3.8 Conclusion . . . 38

4 Superconductivity 40
- 4.1 Mean field free energy . . . 41
- 4.2 Phase diagrams . . . 45
- 4.3 Ginzburg-Landau expansion . . . 48
- 4.4 Discussion . . . 51

5 Summary and Discussions 57

Chapter 1

Introduction

The aim of this thesis is to study the behavior of the high T_c oxide superconducting material on a microscopic model. The novel properties of these materials are the high critical temperature and the appearance of the antiferromagnetic phase very close to the superconducting phase. These properties has been suspected to be due to the strong correlation among electrons. However, the strongly correlated system has long been an unsolved problem of the solid state physics. The difficulty lies in the treatment of the local constraint, that expresses the strong correlation. The *local* nature of the constraint is essential, and therefore, a simple mean field treatment is not adequate.

In this thesis, we take the t-J model, the simplest model of the strongly correlated system, as a microscopic starting point of the study of the high T_c material. We use the slave fermion scheme in this thesis. The local constraint is taken into account by introducing the CP^1 variable (or Schwinger boson) for the spin. Then, the interaction between the hole and the spin arising from the strong correlation is included. Before we start the analysis, we will see in Chap.2 the experimentally known properties of the high T_c material. The properties of the strongly correlated system is intuitively discussed there. The Hamiltonian of the t-J model is given in that chapter and also the previous developments on the t-J model are briefly reviewed. After these preliminaries, the magnetic properties of the material is studied in Chap.3. We start from the anisotropic three-dimensional t-J model taking into the weak three-dimensionality of the high T_c materials. After rewriting the constraint by introducing the CP^1 variable, we derive an effective theory from the t-J model integrating out half of the spins. We calculate the effect of the hole systematically and obtain an effective CP^1 action with the coupling constants renormalized by the hole. Working on this effective action, we can calculate various magnetic properties at small doping. For example, the Néel temperature is obtained as a function of doping. In Chap.4, the superconductivity is studied treating the constraint in the same manner. After rewriting the constraint using the CP^1 variable, the paring force between two holes arising from the strong correlation appears explicitly in the Hamiltonian. We thus perform the mean field analysis of the superconductivity with the nature of the strong correlation taken into account. In Chap.5, we will discuss the remaining problems.

Chapter 2

Preliminaries

2.1 High T_c superconductor

In 1986, superconductivity was observed in a new material, Ba La CuO system[1]. The critical temperature T_c was over 30K, quite higher than the previously known superconductor. What is more important in this discovery is that it opened a possibility of superconductivity in new type of material, Cu oxides. Within one year after that, the highest critical temperature exceeded the liquid nitrogen temperature, and it reached now 125K for Tl oxide[2].

The Cu oxides are originally insulating, and exhibit superconductivity, when some impurities are added. The density of the extracted electrons (i.e. holes), δ, is called the doping ratio. For example, one of these materials, La_2CuO_4, is an insulator at $\delta = 0$ and also has Néel (or long range antiferromagnetic(AF)) order below the Néel temperature T_N (see Fig.2.1). This phase is called the antiferromagnetic phase. If some small fraction δ of La is replaced by other elements M, such as Ca,

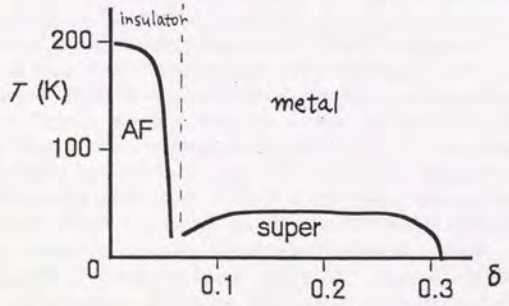

Figure 2.1: The phase diagram of the high T_c material $La_{2-\delta}M_\delta CuO_4$. δ is the doping ratio.

Sr, Ba, the Néel temperature of the resulting material $La_{2-\delta}M_\delta CuO_4$ decreases

and finally vanishes at $\delta \simeq 0.05$. The superconductivity starts immediately after the long range antiferromagnetic order vanishes;i.e. for $\delta \gtrsim 0.05$. Or there may be another phase like spin glass between these phases. The superconductivity ends at $\delta \simeq 0.3$. For larger doping, the material is an usual metal.

In the conventional BCS theory, the superconductivity is explained by the condensation of the electron pairs(Cooper pairs) formed because of the electron-phonon interaction. Since this interaction is weak, the critical temperature has been believed to be no more than ~40K within this mechanism. It appears, therefore, that other mechanism than the pairing by phonon interaction is needed for the high T_c superconductivity. In fact, the isotope effect of the high T_c materials is too small to explain the oxide superconductivity by phonons only[3].

What, then, is responsible for the superconductivity? Let us look into the structure of the oxide superconductor shown in Fig.2.2. The distinct feature of the

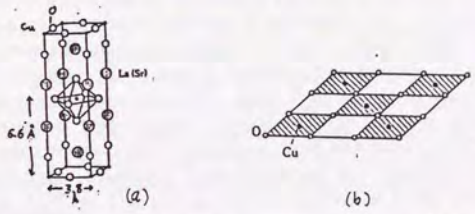

Figure 2.2: (a) The structure of La_2CuO_4. (b) The Cu and O form a two-dimensional network.

structure is that it is quasi two-dimensional: The lattice constant in the z-direction is about $2 \sim 3$ times as large as that in the x- or y-direction. This difference is important, since this can cause a difference by a factor of $\exp(-4 \sim 9)$ in the overlap integrals of the electron wave function. The two-dimensional network made of Cu and O atom is common to all the high T_c materials and accordingly is expected to be essential to the superconductivity.

Let us examine this network from the electronic point of view. The Cu atom in La_2CuO_4 has nine electrons in its $3d$ orbit. The highest band of his orbit is accordingly occupied by one electron. This situation is called the half filling, since each band is filled up by two electrons with spin up and down. Upon doping of one atom of Sr, for instance, one La^{3+} is replaced by Sr^{2+} and consequently one electron is removed from the Cu-O network, or in other words, a hole is created, and the system deviates from the half filling.

Thus the electron model near half filling in the quasi two-dimensional lattice (of Cu atom) is expected to describe the high T_c material. The usual fermi liquid model, however, will not do, since the insulating properties outside the antiferromagnetic phase (i.e. $T > T_N$) are not described well by this model.

We will discuss in the next section what kind of model can explain the antiferromagnetic phase and consequently is suitable for the study of superconductivity.

2.2 High T_c material as strongly correlated system

As mentioned in the previous section, one of the most important properties of high T_c materials is that the superconducting phase is in touch with or very close to the antiferromagnetic insulator phase. What is more, very far from the antiferromagnetic phase(at $\delta \simeq 0.3$), the superconductivity also breaks down (Fig.2.1). This fact naturally makes us to suspect that the origin of the superconductivity is the antiferromagnetic spin interaction. Therefore, one had better begin with the antiferromagnetic phase, before the study of the high T_c superconductivity.

The antiferromagnetic insulator phase is understood easily from the point of view of strongly correlated electron system at half filling. The strong correlation between electrons is due to the short range part of the Coulomb force. The long range part is screened. This correlation is modeled by introducing a large repulsion energy U (> 0) which works when two electrons are on the same site. At half filling, just as in the case of undoped high T_c materials, each site is occupied by exactly one electron in the large U limit. The electrons cannot move, avoiding double occupancy, even though the hopping amplitude t is finite. The system is thus an insulator (called the Mott insulator). The magnetic interaction arises in this situation, through the perturbation of hopping t. Actually, the energy of the neighboring spins is lowered by an amount $J/2 \equiv 2t^2/U$ when the spins point in the opposite direction because of the virtual process depicted in Fig.2.3. Therefore, the antiferromagnetic insulating phase is very natural for the strong

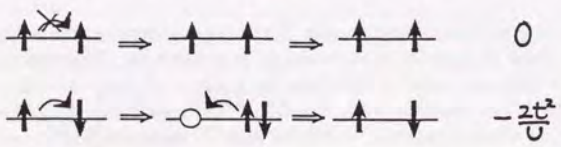

Figure 2.3: The antiferromagnetic interaction $J = 4t^2/U$ arises through the second order process in the Mott insulator.

correlated system at half filling.

On the other hand, without the strong correlation, the electrons in the half filled band move freely and the system becomes an usual metal outside the antiferromagnetic phase.

The experimental fact[4] that the Hall coefficient of doped high T_c materials is positive at small doping (before superconducting phase ends) also supports the strongly correlated nature, since it indicates that the dynamical variable in the system is not the electron but the hole (and spin).

What about the superconductivity in the strongly correlated system? To see the possibility of superconductivity, let us consider classical two holes at a distance in the antiferromagnetic spin background (Fig.2.4(a)). Four of the antiferromag-

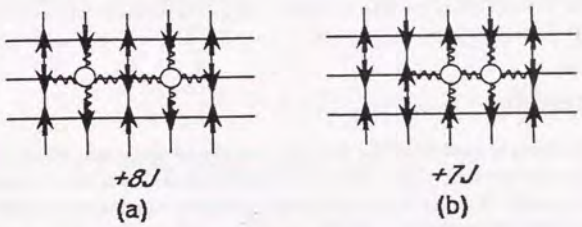

Figure 2.4: Two holes gain energy of J when they are neighboring as in (b) in the antiferromagnetic spin background.

netic bonds couplings (in two-dimensions) are lost because of one hole, and accordingly the energy becomes higher by $8J$ for two holes. If two holes are neighboring (Fig.2.4(b)), however, the energy loss is only $7J$. Thus the magnetic interaction can produce attractive force between holes. This attraction is observed numerically in the exact diagonalization of a small system[5]. Owing to this force, the holes on the neighboring sites will form a pair with charge $+2e$ and the superconductivity will occur by the phenomenological theory of Ginzburg and Landau. The formation of pairs of charge $2e$ is confirmed in the experiments on the Josephson effect and flux quantization[6].

This scenario is, however, too naive. In fact, the antiferromagnetic interaction favors *all* the holes gather together, resulting in the phase separation[7] (Fig.2.5). The remedy is through the hopping term t, since the gathered holes lose much

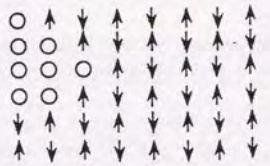

Figure 2.5: Phase separation into the hole(denoted by o)-rich and spin($\uparrow$)-rich part occurs for large J.

kinetic energy due to their immobility. In the real materials, $t \simeq 0.4 \sim 0.5$eV may be said to be large enough compared to $J \sim 0.1$eV. The phase separation is observed numerically for $t/J \lesssim 1 \sim 2$ in the one dimensional t-J model[8]. The hopping term is important also for the superconducting current and the Meissner effect to appear.

From these considerations, our study in this thesis is based on the microscopic model of strongly correlated electrons, which we are going to specify in the next

Section. It is seen in later chapters that the model explains various characteristic properties of high T_c materials well.

2.3 t-J model

Among many microscopic models of the strongly correlated electrons, we choose the t-J[9] model as our starting point. One of the reasons is that it is the simplest. It is a single band model. It contains only two terms, namely, the nearest neighbor electron hopping t and the antiferromagnetic nearest neighbor spin interaction J.

There are other models of strongly correlated system which are more complicated, but is more realistic. For example, it is possible to consider the next nearest neighbor interactions besides nearest neighbor ones. This model, the tt'-JJ' model, is frustrated for $J, J' > 0$, and is important to produce parity breaking ground state. This state is a starting point of the explanation of the superconductivity by anyon. This possibility of superconductivity due to anyon was discussed extensively[10] because of the distinguished two-dimensionality of the material. The experiments are, however, against the anyon superconductivity. For instance, the parity breaking and existence of the strong magnetic field, which necessarily appears in the presence of the anyons, are denied[11].

One can also include the O2p orbit in addition to the Cu3d. This model, d-p model, is more realistic than one band models like t-J, since the hole is observed to be in the O2p orbit by the photoemission experiments[12]. However, it is argued[13] that the doped hole in O2p orbit forms a singlet with a hole in Cu3d orbit, owing to the strong antiferromagnetic interaction $J_K (\simeq 0.5 \sim 1\text{eV})$ between holes in these two orbit. This singlet in the d-p model can be regarded as the hole in the t-J model, and thus the d-p model may reduce to the t-J model for large J_K.

We expect, in spite of the fascination of these realistic models, that the essential features of the antiferromagnetic and the superconductivity are contained in the simple t-J model.

The Hubbard model is also very simple, but in numerical simulations[14], no tendency of superconductivity is observed, while the attractive force between holes is seen in the case of the t-J model. The Hubbard model also reduces to the t-J model with $J = 4t^2/U$ in the limit of large Coulomb repulsion U (i.e., $J \ll t$)[15], although this equivalence does not hold for finite U.

We consider the t-J model on three-dimensional square lattice with anisotropy. (We use the term "dimension" only for the spatial ones.) In real materials, the structure is not exactly the square lattice as shown in Fig.2.2(a). However, this approximation by the square lattice is expected not to change the low energy behaviors of the model.

Hamiltonian of t-J model The t-J model is the lattice model of electron $c_{x\sigma}$ with spin $\sigma = \uparrow$ or $\downarrow$. The hopping amplitude of the electron to nearest neighbor

site is denoted by t and the nearest neighbor antiferromagnetic interaction is J:

$$\begin{aligned} H_{t-J} &= -t \sum_{x,\mu} \sum_{\sigma} (1 - n_{x,-\sigma}) c^{\dagger}_{x\sigma} c_{x+\mu,\sigma} (1 - n_{x+\mu,-\sigma}) \\ &\quad + \frac{J}{2} \sum_{x,\mu} \left(\vec{S}_x \cdot \vec{S}_{x+\mu} - \sum_{\sigma} \frac{1}{4} n_{x\sigma} n_{x+\mu,\sigma} \right) - \mu_c \sum_{x\sigma} n_{x\sigma}, \end{aligned} \tag{2.1}$$

where the spin $\vec{S}$ is written using the Pauli matrix $\vec{\sigma}$,

$$\vec{S}_x = \frac{1}{2} c^{\dagger}_x \vec{\sigma} c_x, \tag{2.2}$$

and $\mu = \pm 1, \pm 2$. The term $(1/4) n_{x\sigma} n_{x+\mu,\sigma}$ is added in this thesis to make the calculation easier. This factor does not change the results very much. The parameters are $t \simeq 0.4 \sim 0.5$ eV and $J \simeq 0.1$eV according to experiments. The chemical potential μ_c is determined so as to fix the hole density to be doping δ:

$$1 - \delta = \sum_{\sigma} < n_{x\sigma} > . \tag{2.3}$$

The physical space of this Hamiltonian is restricted to no doubly occupied states at each site: $|0>, |\uparrow>, |\downarrow>, (\text{no } |\uparrow\downarrow>)$. The factor $(1 - n_{x,-\sigma})$ in the hopping term enforces this constraint on each hopping. Although the Hamiltonian appears to be simple, the constraint of no double occupancy makes the t-J model complicated. However, the essence of the strongly correlated nature is reflected through this local constraint. For example, if we simply replace the factor $(1 - n_{x,-\sigma})$ by an average value, $\delta/2$, we cannot produce the insulating properties(see Sect.2.2). The most important thing, therefore, in dealing with the t-J model is to take into account this constraint in a local form as it is. For this purpose, the introduction of the auxiliary boson is useful.

Local constraint and auxiliary boson As stated above, the treatment of the local constraint is essential although difficult in the t-J model. One of the way to take this constraint into consideration is the Guzwiller approximation[17], suitable for the numerical calculations[18]. In analytical approaches, the introduction of the auxiliary boson[16] is convenient to respect this constraint. The electron operator is written in this method as a product of spin and hole operators. In the slave boson representation, the spin and the hole is expressed by a fermion $f_{x\sigma}$ and a boson b_x, respectively:

$$c_{x\sigma} = b^{\dagger}_x f_{x\sigma}. \tag{2.4}$$

This equation states that annihilating an electron in the space of no double occupancy is to annihilate a spin $f_{x\sigma}$ and create a hole $b^{\dagger}_x$. Since additional bosonic degrees of freedom is introduced, a constraint is needed to reproduce the commutation relation of the electron operator:

$$b^{\dagger}_x b_x + \sum_{\sigma} f^{\dagger}_{x\sigma} f_{x\sigma} = 1. \tag{2.5}$$

This constraint is equivalent to the condition of no double occupancy. Since we have divided the electronic degrees of freedom into those of the hole and spin, there arises an U(1) gauge invariance:

$$\begin{aligned} f_{x\sigma} &\to f_{x\sigma} e^{i\theta_x} \\ b_x &\to b_x e^{i\theta_x}. \end{aligned} \tag{2.6}$$

The physical quantity must be invariant under this transformation.

The reinterpretation of the electron system in the language of hole and spin is very natural in the present situation. Actually, at small doping, almost all sites are occupied by an electron. If an electron at x is to hop to nearest neighbor site, $x+\mu$, the site $x+\mu$ must be vacant(i.e., occupied by a hole), because of the factor $(1-n_{x-\sigma})$ in the hopping term(See Fig.2.6). The hole hopping, on the

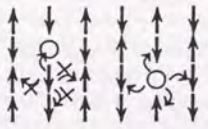

Figure 2.6: Strongly correlated electron can hop only if the nearest neighbor site is vacant, while the hole hops without much restriction at small doping.

other hand, is not restricted by the strong correlation very much. This is because, although holes are also forbidden to be doubly occupied(due to eq.(2.5)), they are very rare to come across each other at small hole density. Thus from the form of the hopping term the hole degree of freedom is a better variable than the electron operator itself in the high T_c material. This is consistent with the experiment that shows that the charge carrier of the material has positive sign[4].

It is also possible to write hole and spin by fermion ψ_x and boson $a_{x\sigma}$, respectively.

$$c_{x\sigma} = \psi_x^\dagger a_{x\sigma} \tag{2.7}$$

This scheme is called the slave fermion representation. The constraint is

$$\psi_x^\dagger \psi_x + \sum_\sigma a_{x\sigma}^\dagger a_{x\sigma} = 1. \tag{2.8}$$

The gauge invariance arises in the similar way as eq.(2.6). Both representation, slave-boson and -fermion, must give the same result as the original t-J model (2.1), if the constraints are faithfully respected.

In the next section, we review briefly the previous developments in the study of the t-J model.

2.4 Previous approaches to t-J model

Mean Field theories The common technique in solving the t-J model is the mean field (or Equivalently the large N) treatment. There have been so many mean field theories of two-dimensional t-J model using different order parameters. Before starting the mean field analysis on the superconductivity in Sect.4, we need to examine what kind of mean field theory have been already done and what has not. In table 2.1, some of the mean field theories are listed almost in the historical order. The early mean field theories (I) studied the condensation of the

	order parameter			ref.
(I)	electron RVB	$c_{x\uparrow}c_{y\downarrow} - c_{x\downarrow}c_{y\uparrow}$	electron	[19] [20]
(II)	spin RVB spin hopping	$f_{x\uparrow}f_{y\downarrow} - f_{x\downarrow}f_{y\uparrow}$ $f_x^\dagger f_y$	slave boson	[21]
(III)	spin RVB hole&spin hopping	$a_{x\uparrow}a_{y\downarrow} - a_{x\downarrow}a_{y\uparrow}$ $\psi_x^\dagger\psi_y$, $a_{x\sigma}^\dagger a_{y\sigma}$	slave fermion spiral state	[22]
(I')	electron hopping	$\sum_\sigma^N c_{x\sigma}^\dagger c_{y\sigma}$	large N	[23]

Table 2.1: mean field theories of t-J model. The operators are, $c_{x\sigma}$:electron, spin fermion in the slave boson representation:$f_{x\sigma}$, spin boson in the slave fermion :$a_{x\sigma}$ and the hole fermion:ψ_x.

nearest neighbor electron singlet operator. This operator is called the resonating valence bond (RVB) operator, and is originally introduced by Anderson to describe the antiferromagnetic spin system with large fluctuation (e.g., antiferromagnetic Heisenberg model on one- or two-dimensional triangular-lattice). In the RVB state at low temperature, this operator has nonvanishing expectation value. According to refs.[9,19], the superconductivity occurs when these condensed RVB pairs begin to flow at finite doping. The magnetic phase was not discussed in the mean field theory[19]. In addition, the ground state ($T=0$) of two dimensional Heisenberg model, equivalent to the t-J model at $\delta = 0$, was found numerically to be the Néel ordered state[24]. That is, the short range (nearest neighbor) RVB operator is not a good order parameter of magnetic order at small doping.

Later, the order parameter of spin hopping besides RVB operator was included (II) using the slave boson representation, so as to study possibly other phase than the magnetic one. In fact, the superconductivity was discussed in this approach by the simultaneous condensation of the RVB operator and the hole boson, namely, by $< f_{x\uparrow}f_{x+\mu,\downarrow} - f_{x\downarrow}f_{x+\mu,\uparrow} >< b_x^\dagger b_{x+\mu}^\dagger > \neq 0$. The slave boson is essential in this scenario, since nonvanishing $< b_x^\dagger b_{x+\mu}^\dagger >$ was given by the bose condensation of holes $< b_x^\dagger > \neq 0$. It appears, however, necessary to introduce the order parameter of the superconductivity itself (not as a product of two order parameters) in order to discuss the superconductivity.

In these mean field analyses, the non uniform (non S wave) configurations of

the μ-dependent order parameter $\Delta_{x\mu}$) are favored in some cases to the S wave one ($\Delta_{x,\mu}$ =constant). For the RVB order parameter of the fermionic spin, d-wave solution $\Delta_1 = -\Delta_2$ was shown to be stable[21]. The systematic study(I') of the non uniform solution within the periodicity of $\sqrt{2}a$ (with lattice constant a) was done in [23]. The order parameter is in the electron hopping channel. This mean field is justified in the large N (where $\sigma = 1 \sim N$, $N = 2$ for $S = 1/2$) limit, and has nothing to do with the superconductivity. Assuming this periodicity, four of the order parameters $\Delta_i (i = 1 \sim 4)$ are independent (Fig.4.2). The non uniform ground state with flux π (that is, $\Delta_1\Delta_2\Delta_3\Delta_4 = |\Delta|^4 e^{i\pi}$) is found for some parameter region, and this state was named the "flux state".

Concerning the difference of the slave-boson and slave-fermion scheme, the slave fermion one is found to give lower ground state energy in the mean field theory than the slave boson one[25]. The resulting energy, however, becomes much lower than the exact value. It has been difficult to study the superconductivity in the slave fermion theory, since the attraction of hole fermion appears explicitly only after the local constraint (2.8) is solved. As a result, the mean field theories thereafter are mainly concerned with the spin configuration in the presence of dynamical hole (III).

In (III), the order parameter in the hole hopping channel is included besides the two in (II). In these slave fermion mean field theories, so called the (1,1)-spiral state[26] is obtained as the ground state. The characteristic feature of this state is the following behavior of the correlation function.

$$< \vec{S}_x \vec{S}_y > \propto \cos 2\vec{k}_0(\vec{x} - \vec{y}), \tag{2.9}$$

where $\vec{k}_0 \equiv k_0(1,1)$. Within the slave fermion mean field theories, this state has a long range order (i.e., the two point function (2.9) does not decay at long distance) at zero temperature, owing to the Bose condensation of the spin boson $a_{x\sigma}$. At zero doping, $k_0 = \pi/2$, which is the usual Néel order. As holes are doped, the Néel order is disturbed more and more with the growth of the hole hopping amplitude $< \psi_x^\dagger \psi_{x+\mu} > \propto \delta$. As a result, the orientation of spins rotate spatially (see Fig.4.1). In the mean field solution, this spiral configuration is expressed by the deviation of k_0 from $\pi/2$,

$$k_0 = \frac{\pi}{2} - Q(\delta), \tag{2.10}$$

and the pitch Q of rotation is proportional to doping in mean field theory

$$Q = (0.2 \sim 1.2) \times \frac{t}{J}\delta. \tag{2.11}$$

The *short range* spiral (or incommensulate) configuration of the spin is observed at $\delta = 0.07$ in the neutron scattering experiment[27], although no kind of *long range* magnetic order is observed outside the antiferromagnetic phase. (Recently, it is also reported[28] that the configuration realized in the real La-superconductor is the short range spiral state with the pitch $k_0 \times (1,0)$, not (1,1)).

The spiral state allows the band motion of the hole, and thus is a good background spin configuration for the superconductivity (see Sect.4).

Let us stress that in all the mean field theories above, the constraint is taken into account only globally. That is, the constraint is included by a Lagrange multiplier λ_x, but only the constant solution is looked for: $\lambda_x = \lambda$(constant). In this treatment of the constraint, the state with many bosons at one site is not excluded, and thus the dynamics is changed very much. The local nature of the constraint is included gradually if the fluctuation around the mean field solution is treated dynamically in a systematic $(1/N)$ manner. The fluctuation behaves as a gauge field of U(1) gauge transformation (2.6). The mean field treatment becomes exact in the large N analysis (I').

CP^1 approach at zero doping As mentioned in Sect.2.1, the antiferromagnetic phase is very important in understanding the high T_c superconductor. Hence, it is very useful to investigate the magnetic properties of the high T_c material.

At zero doping, the hopping vanishes, and the t-J model reduces to the antiferromagnetic Heisenberg model. This model has been studied a lot, and its continuum limit after half of the spins integrated out is the CP^1 σ model[29]. The constraint reduces at zero doping to the requirement on the length of the spin. In the continuum theory, the renormalization group analysis is easy. Ref.[30] showed by this technique that the two dimensional CP^1 model well describes the experimental results on undoped La_2CuO_4. The constraint was imposed globally. Since it deals with the two dimensional model, the quantities very sensitive to the weak three-dimensionality can not be reproduced. For example, the Néel temperature T_N vanishes owing to the infrared divergence in two-dimensions, in accordance with the theorem of Mermin and Wagner[31]. Also, the holes are not included, and an important question of how the Néel temperature lowers as doping increases could not be answered.

Other approaches In the numerical studies of the two dimensional t-J model, the attractive force between two holes is observed by the exact diagonalization of a small cluster[5], However, the system size available is very small, for instance, 4×4 sites, and accordingly the results are not necessary reliable.

The one dimensional t-J model is exactly solvable at $t = J$ using the Bethe ansatz[32], and its study may help us to understand the two dimensional one. The exact solution indicates that the spin and the charge degrees of freedom are decoupled and each behaves like a free fermion. This is called the charge-spin separation. In the ground state solution, the momentum distribution of the electron is smooth at the fermi momentum k_F. This behavior is different from that of the normal fermi liquid, which has a finite discontinuity there. The system with this property is called the Luttinger liquid[33]. It might be expected that the two dimensional t-J model has a similar non fermi liquid behavior, and that this might explain the anomalous properties of the normal state of the high T_c materials.

2.5 Our formalism

As already noted, the essence of the strong correlation is in the local constraint in the t-J model. In the previous analytical approaches, however, this constraint has not been included locally. In this thesis, we will study the t-J model taking into account to some extent the local nature of the constraint.

The interaction arising from the local constraint is included if the constraint is rewritten using the new spin variable[34]. This new variable, the Schwinger boson, $z_{x\sigma}$ is defined by

$$a_{x\sigma} = (1 - \psi_x^\dagger \psi_x)^{1/2} z_{x\sigma}. \tag{2.12}$$

The projection factor $(1-\psi_x^\dagger\psi_x)^{1/2}$ represents the local contraction of the spin due to the presence of holes. This projection is well defined since the particle number of fermions is 0 or 1. It also guarantees that the field $z_{x\sigma}$ becomes meaningless when the site is occupied by a hole ψ_x. In terms of $z_{x\sigma}$, the constraint (2.8) becomes

$$z_{x\sigma}^\dagger z_{x\sigma} = 1. \tag{2.13}$$

This is the CP^1 constraint. The fermion ψ_x is now free of constraint. Therefore, the interaction between the hole and the spin arising from the strong correlation—in particular, the attractive force between nearest neighbor holes—can be explicitly seen after this transformation (see (4.3)). If an approximation (like mean field) is made after this transformation, the essential part of the hole-spin interaction arising from the local constraint is expected to be taken into account.

Let us note that this transformation is not possible in the slave boson scheme. This is because the $< 1 - b_x^\dagger b_x >$ can be negative for bosonic field b_x, and accordingly the projection $(1 - b_x^\dagger b_x)^{1/2}$ is not well defined.

In the following chapters, we use this transformation for studying the properties of the high T_c material, and will see that they are reproduced well. In this thesis, the constraint (2.13), which no longer contains the explicit interaction between spin and hole, is treated by a mean field. This constraint would become important in discussing the fermi surface of the system in the slave fermion scheme (see Chap.5).

Chapter 3

Magnetic properties

In this chapter, we study the magnetic properties of the high T_c material. These properties are important for the study of the superconductivity. This chapter is based on Ref.[35].

We extend the analysis on the CP^1 model[30] to the doped region and also to the (weakly) three-dimensional case to produce the finite Néel temperature. The inclusion of the hole is done by deriving an effective theory from the t-J model by solving the constraint by eq.(2.12) and then integrating out half of the spins. We assume in this derivation the short range antiferromagnetic order and small doping. The resulting effective theory is the anisotropic three dimensional CP^1 model coupled with hole fermions. On this effective theory, we can study the effects of doping systematically. At small doping, the effective theory reduces to the CP^1 model with coupling constants renormalized by holes. Once the effective theory is derived, the CP^1 constraint is treated by mean field, since this constraint does not produce the interaction between the spin and hole anymore. Various physical quantities are calculated in the mean field approximation. Our interest is mainly in the effects of weak three-dimensionality and of hole doping. The decrease of the Néel temperature due to the hole is estimated quantitively. We will also study the spiral state outside the antiferromagnetic region on our effective model.

3.1 Derivation of the effective theory

As mentioned in Sect.2.1, the distance between the nearest Cu-O planes in real high T_c materials is about twice as large as the distance between the nearest two Cu atoms in the Cu-O plane. Because of this, electrons at Cu atoms in different planes have smaller overlap integral, and the electron hopping amplitude and the magnetic interaction is very small in the direction perpendicular to the Cu-O planes (we call it the third direction).

We therefore start from the following three-dimensional t-J model with anisotropy in the slave-fermion representation,

$$\hat{H}_{t-J} = \sum_{x,\pm\mu} t_\mu \hat{\psi}_x^\dagger \hat{a}_{x\pm\mu}^\dagger \hat{a}_x \hat{\psi}_{x\pm\mu}$$

$$+ \sum_{x,\mu} \frac{J_\mu}{4} \left[(\hat{a}^\dagger \vec{\sigma} \hat{a})_x (\hat{a}^\dagger \vec{\sigma} \hat{a})_{x+\mu} - (\hat{a}^\dagger \hat{a})_x (\hat{a}^\dagger \hat{a})_{x+\mu} \right]$$
$$-\mu_c \sum_x (\hat{a}^\dagger \hat{a})_x \tag{3.1}$$

The slave fermion representation of the t-J model is convenient, since the bosonic spin variable can later be naturally interpreted as the CP^1 variable. The weakness of the couplings in the third direction is represented by a factor of $\alpha(\leq 1)$:

$$t_\mu(\mu = 1,2,3) = t(1,1,\sqrt{\alpha})$$
$$J_\mu = J(1,1,\alpha). \tag{3.2}$$

Here, the anisotropy of t_μ is chosen to be $\sqrt{\alpha}$ in accordance with the t-J model derived from the Hubbard model. The results, however, do not change very much by the choice of the α-dependence of t_3/t, if this ratio is small. The anisotropic parameter α will be estimated to be of order 10^{-5} in the later investigation.

The lattice spacing of the Cu-O plane (we call it $X-Y$ plane) is a and that of the third direction is a_3, and $a_3 = \lambda^{\frac{1}{2}} a$ with $\lambda^{\frac{1}{2}} \sim 2$ (the actual values of a and a_3 will be given in Sect.3.5).

As stated already, the above t-J Hamiltonian is defined on the Hilbert space without doubly occupied states, which fact is expressed by the local constraint

$$\hat{\psi}_x^\dagger \hat{\psi}_x + \sum_\sigma \hat{a}_{x,\sigma}^\dagger \hat{a}_{x,\sigma} = 1. \tag{3.3}$$

The constraint (3.3) contains both bosons and fermions. It is convenient, as mentioned in Sect.2.3, to introduce the bosonic CP^1 operator $\hat{z}_{x,\sigma}$ and the projection operator $\hat{\rho}_x$ to make the fermion free of constraint,

$$\begin{aligned} \hat{a}_{x,\sigma} &\equiv \hat{\rho}_x \hat{z}_{x,\sigma} \\ &= (1 - \hat{\psi}_x^\dagger \hat{\psi}_x)^{1/2} \hat{z}_{x,\sigma}, \end{aligned} \tag{3.4}$$

where

$$\hat{\rho}_x^2 \equiv 1 - \hat{\psi}_x^\dagger \hat{\psi}_x \tag{3.5}$$

In terms of the z-field, the constraint (3.3) becomes that of CP^1,

$$\sum_\sigma \hat{z}_{x,\sigma}^\dagger \hat{z}_{x,\sigma} = 1, \tag{3.6}$$

and the Hamiltonian takes the form

$$\begin{aligned} H_{tJ} &= t \sum_{x,\mu} (\psi_{x+\mu}^\dagger a_x^\dagger a_{x+\mu} \psi_x + h.c.) + \mu_c \sum_x (\psi^\dagger \psi - 1)_x \\ &+ \frac{J}{2} \sum_{x\mu} \rho_x^2 \rho_{x+\mu}^2 \left(|z_x^\dagger z_{x+\mu}|^2 - 1 \right). \end{aligned} \tag{3.7}$$

We use the path-integral formulation of finite-temperature quantum many-body system. In the present case, the partition function is given by

$$Z = \int [Dz D\psi] \delta\Big(\sum_\sigma \overline{z}_{x,\sigma} z_{x,\sigma} - 1 \Big) J_{\rm gf}$$
$$\times \exp\Big\{ \int_0^\beta d\tau \Big[- \sum_x \Big(\sum_\sigma \overline{a}_{x,\sigma} \dot{a}_{x,\sigma} + \overline{\psi}_x \dot{\psi}_x \Big) - H_{t-J} \Big] \Big\} \tag{3.8}$$

In eq.(3.8), $z_{x,\sigma}(\tau), \overline{z}_{x,\sigma}(\tau)$, are complex variables, while $\psi_x(\tau), \overline{\psi}_x(\tau)$ are Grassmann variables. The bars indicate conjugate quantities. The imaginary time τ runs from 0 to β. The substitution $a_{x,\sigma}(\tau) = \rho_x(\tau) z_{x,\sigma}(\tau)$, $(\rho_x = (1 - \overline{\psi}_x \psi_x)^{1/2})$ is understood. H_{t-J} is obtained from $\hat{H}_{t-J}$ by replacing operators $(\hat{z}_\sigma, \hat{z}_\sigma^\dagger, \hat{\psi}, \hat{\psi}^\dagger)_x$ by $(z_\sigma, \overline{z}_\sigma, \psi, \overline{\psi})_x(\tau)$. The constraint (3.3) is guaranteed by the δ-function in eq.(3.8). The factor $J_{\rm gf}$ reflects the Jacobian associated with the gauge fixing into the smooth configurations of $z_x(\tau)$'s. Explicitly it reads $J_{\rm gf} = \prod_{x \in \text{sublattice}} \prod_\tau \exp(-\bar{\psi}_x(\tau)\psi_x(\tau))$ (see Appendix A of ref.[34]). It is necessary to obtain a reasonable continuum field theory as a low-energy effective theory. The system has (at least) short range

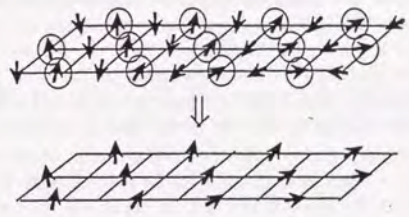

Figure 3.1: In the short range antiferromagnetic configuration, the spins on the same sublattice are in the smooth configuration. Hence the continuum limit exists after integrating out one of the sublattices marked by ◯.

antiferromagnetic order, because of the J-term. Actually, it is read from eq.(3.7) that in the language of CP^1 variables, the favored configuration at small doping(i.e. $\rho_x^2 \simeq 1$) is that with short range antiferromagnetic order,

$$\bar{z}_x z_{x+\mu} \simeq 0. \tag{3.9}$$

This indicates that, if we divide the lattice into two sublattices (even(e) and odd(o)), the spins on, say, even lattice (we call it e-spin) are in the smooth configuration (see Fig.3.1). The short range antiferromagnetic order is observed to exist for the length of 200Å even at room temperature in the neutron scattering experiment[36]. Integrating out the o-spins, therefore, we can derive the effective theory of e-spin and holes on both e- and o-sites, and also be able to take the continuum limit of the theory. Parametrization of the o-spin needed for integration is carried out as follows.

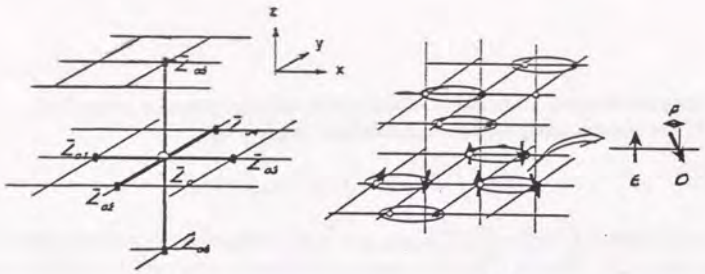

Figure 3.2: (a): Each odd site o has 6 even-site neighbors. They are numbered from 1 to 6. The spins and holes on those even sites are named z_{oi} and ψ_{oi} $(i = 1 \sim 6)$. (b):We pair up each odd-site spin z_o at $o = (x_1, x_2, x_3)$ with a nearest neighbor even-site spin z_e sitting at the left hand side $e = o - \hat{1} = (x_1 - 1, x_2, x_3)$. Two spins in a pair tend to point to the opposite direction due to the antiferromagnetic coupling.

For each site in e-sublattice, there are 6 nearest neighbor o-sites. We number them from 1 to 6 as shown in Fig.3.2(a) , and denote the spins and holes on these sites as z_{oi} and ψ_{oi} (o = some specific odd site, $i = 1, \cdots, 6$ denotes six nearest neighbor even sites), respectively. As the correlation in the X-Y plane is much stronger than the interplane correlation, we pair up each odd site spin with a nearest neighbor even site spin in the $X - Y$ plane. Let us focus on some specific odd spin z_o at $o = (x_1, x_2, x_3)$, and denote the even site spin of its partner sitting on the left hand side $o - \hat{1} = (x_1 - 1, x_2, x_3)$ as z_e ($e \equiv o - \hat{1}$. See Fig.3.2(b)).

Since the space of the CP^1 variable ($\bar{z}z = 1$) is expanded by z and $\tilde{z}$, where $\tilde{z}$ is the reversed spin variable (i.e. $\tilde{z}\vec{\sigma}\tilde{z} = -\bar{z}\vec{\sigma}z$)

$$\tilde{z} = \begin{pmatrix} \bar{z}_2 \\ -\bar{z}_1 \end{pmatrix}, \tag{3.10}$$

the odd spin z_o is parametrized by even spin partner z_e and $\tilde{z}_e$ on the left hand side using two complex numbers p_o and q_o with unit length ($|p_o|^2 + |q_o|^2 = 1$) as

$$z_o = p_o z_e + q_o \tilde{z}_e. \tag{3.11}$$

Complex number p_o represent the fluctuation from the short range antiferromagnetic order (Fig.3.2(b)). Substituting eq.(3.11) into the path-integral representation of the partition function, we integrate over the complex variables p_o and q_o under the constraint $|p_o|^2 + |q_o|^2 = 1$.

The integral, according to eq.(3.9), is dominated by the configuration of small $|p_o|$. We can thus expand the integrand in powers of p_o and $\overline{p}_o$, take up to the quadratic terms, and do the Gaussian integral over p_o and $\overline{p}_o$. Careful estimation[34] shows that the neglected terms are the higher order of $(\beta J)^{-1}$.

It is important to notice that the assumption of the *short range* antiferromagnetic order is different from the *long range* antiferromagnetic (Néel) order. Our

effective theory is therefore applicable to the study of states without long range antiferromagnetic order, for example, of spiral state and superconducting state(see Sects.3.7, 4.4).

Here we give the final result of that integration over all z_o's on odd sites. Detailed derivation is given in ref. [34].

The slave boson-fermion formalism has an invariance under the following local phase (gauge) transformation,

$$(z_\sigma, \psi)_x \to e^{i\theta(x)}(z_\sigma, \psi)_x \tag{3.12}$$

From eq.(3.11), p_o and q_o transform nontrivially under eq.(3.12), and especially for q_o,

$$\begin{aligned} q_o &\equiv \sqrt{1 - |p_o|^2}\, U_{oe} \\ U_{oe} &\to U_{oe} \exp(i(\theta(o) + \theta(e)) \end{aligned} \tag{3.13}$$

After integration over p_o, we find that U_{oe} in the effective action disappears when one introduce the following fermion field on odd sites,

$$\eta_o \equiv U_{oe}\overline{\psi}_o \tag{3.14}$$

this η_o transforms like z_e under (3.12). The even site fermions are written simply as ψ. Using these notations, the partition function reads (dropping the subscript e of the spin)

$$Z = \int [DzD\psi D\eta]\delta(\bar{z}z - 1)\exp(-A), \tag{3.15}$$

where the effective action A is

$$A = A_0 + K_0 + T_{\rm hop} + T'_{\rm 4f}, \tag{3.16}$$

and

$$\begin{aligned} A_0 &= \int_0^\beta d\tau \sum_o \left[-\frac{2}{Q}\, \rho_o^2 (\overline{\dot{z}} \cdot \dot{z})(\overline{z} \cdot \dot{\tilde{z}}) - \frac{1}{2} \sum_i \rho_o^2 J_i \rho_{oi}^2 (\overline{z}_{oi} \cdot z)(\overline{z} \cdot z_{oi}) \right. \\ &\quad \left. - \frac{\rho_o^2}{2Q} \sum_{i,j} J_i \rho_{oi}^2 J_j \rho_{oj}^2 (\overline{z}_{oi} \cdot z)(\overline{z} \cdot z_{oj})(\overline{z}_{oj} \cdot \dot{\tilde{z}})(\overline{\dot{z}} \cdot z_{oi}) \right], \\ K_0 &= \sum_i \overline{\psi}_{oi}(\partial_\tau - \overline{z} \cdot \dot{z} + \mu_c)\psi_{oi} + \overline{\eta}_o(\partial_\tau - \overline{z} \cdot \dot{z} - \mu_c)\eta_o \end{aligned} \tag{3.17}$$

with

$$Q = \sum_j J_j \rho_{oj}^2. \tag{3.18}$$

Here, J_i $(i = 1, \cdots, 6)$ takes $J_{1,2,3,4} = J$ and $J_{5,6} = J_z = \alpha J$. Similarly, $t_{1,2,3,4} = t$ and $t_{5,6} = t_z = (\alpha)^{1/2}t$. Summation $\sum_o$ runs over all the odd sites.

After integration over z_o, z_e interact with even sites z_{oi} ($i = 1 \sim 6$) nearest neighbor to the integrated site o, (See Fig.3.3.) The hopping term $T_{\rm hop}$ is

$$T_{\rm hop} = -\int d\tau \sum_o \sum_i t_i (B_i(o)\overline{\psi}_{oi}\overline{\eta}_o + C_i(o)\eta_o\psi_{oi}), \tag{3.19}$$

where $B_i(o)$ and $C_i(o)$ represent the effective hopping amplitude of hole in the short range antiferromagnetic background:

$$\begin{aligned} B_i(o) &= -(\overline{\bar{z}}\cdot z_{oi}) + \frac{1}{2J}(\overline{\bar{z}}\cdot\dot{z})(\overline{z}\cdot z_{oi}) \\ &+ \frac{1}{4J}\sum_j J_j(\overline{\bar{z}}\cdot z_{oj})(\overline{z}_{oj}\cdot z)(\overline{z}\cdot z_{oi}) \\ C_i(o) &= -(\overline{z}_{oi}\cdot\bar{z}) + \frac{1}{2J}(\overline{z}\cdot\dot{\bar{z}})(\overline{z}_{oi}\cdot z) \\ &+ \frac{1}{4J}\sum_j J_i(\overline{z}_{oj}\cdot\bar{z})(\overline{z}\cdot z_{oj})(\overline{z}_{oi}\cdot z), \end{aligned} \tag{3.20}$$

(for $\alpha \ll 1$).

It is read from these expressions that the hole hopping from the site o to e is possible when the expectation value $< \bar{\bar{z}} z_{oi} >$ is non vanishing, namely, when the antiferromagnetic order of the spin is locally destroyed.

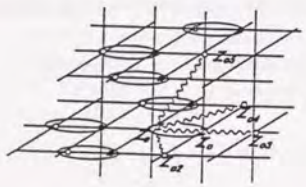

Figure 3.3: After integrating out the odd site spin z_o, its partner z_e interacts with the even spins z_{oi} neighboring to z_o.

The term T'_{4f} is a four fermi term:

$$T'_{4f} = -\frac{1}{2J}\int d\tau \sum_o \sum_{i,j} t_i t_j \eta_o\psi_{oi}\bar{\psi}_{oj}\bar{\eta}_o(\bar{z}_{oi}z)(\bar{z}z_{oj}). \tag{3.21}$$

This, together with the other four fermi terms in A_0, play an important role in the superconducting state. Higher order fermion interactions are neglected, since we consider small doping region.

The action (3.16) is complicated and at a glance appears to lack rotational invariance. However, careful investigation shows that eq.(3.16) is isotropic. In fact, we see later that the continuum limit of A at small doping is relativistically invariant CP^1 action(see eq.(3.36)).

3.2 Effective CP^1 action

For the study of the small doping region, we need further to pick up relevant terms in A. Let us first read from the action (3.16) the free spin part. This part is obtained by the tree level replacement(or Hartree approximation), $\bar{\psi}\psi, \bar{\eta}\eta \to \delta$ in A_0, that is,

$$\begin{aligned} A_0^{\rm tr}(\bar{z}, z, \delta) &\equiv A_0(\rho \to (1-\delta)^{\frac{1}{2}}) \\ &\equiv \int_0^\beta d\tau \sum_{o\in{\rm odd}} \left[-\frac{1}{(2+\alpha)J}(\overline{\bar{z}}\cdot\dot{z})(\overline{z}\cdot\dot{\bar{z}}) - \frac{(1-\delta)^2}{2}\sum_i J_i(\overline{z}_{oi}\cdot z)(\overline{z}\cdot z_{oi}) \right. \\ &\left. - \frac{(1-\delta)^2}{4(2+\alpha)J}\sum_{i,j} J_i J_j (\overline{z}_{oi}\cdot z)(\overline{z}\cdot z_{oj})(\overline{z}_{oj}\cdot\bar{z})(\overline{\bar{z}}\cdot z_{oi}) \right]. \end{aligned} \tag{3.22}$$

The free part of fermion is given by $K_0 + A_0$ with spins replaced by the expectation values at antiferromagnetic order(i.e., setting $\bar{z}z_{oi} \simeq 1, \bar{z}\dot{z} \simeq 0$ etc.). The fermion mass μ_c is shifted by this decoupling to be

$$m = \mu_c + (2+\alpha)J. \tag{3.23}$$

The free part of the fermion is thus

$$K(\psi,\eta) = \int_0^\beta d\tau \sum_o \left[\sum_i \overline{\psi}_{oi}(\partial_\tau + m)\psi_{oi} + \overline{\eta}_o(\partial_\tau - m)\eta_o \right]. \tag{3.24}$$

We next examine the interaction terms between the hole and the spin. One of our main aim in this chapter is to study how the holes destroy the antiferromagnetic order, and consequently, lower the Néel temperature. For this purpose, the most important interaction term is expected to be the hopping term $T_{\rm hop}$. Naively speaking, hole hopping destroys the antiferromagnetic order as shown in Fig.3.4.

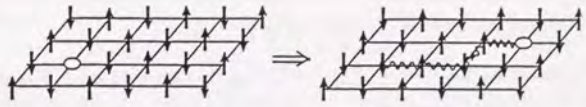

Figure 3.4: The antiferromagnetic order is destroyed along the trail of hole hopping.

This fact is also read from the expression of B_i and C_i in eq.(3.20). Since the amplitude of hopping is small in the presence of short range antiferromagnetic order, we can treat the term $T_{\rm hop}$ by a perturbation.

There are other terms: T'_{4f} and four- and higher-fermi interactions arising from A_0 through ρ. They work as an attractive forces between neighboring holes. These

forces are essential in formation of superconducting hole pairs(see Chap.4), but would have little effect on antiferromagnetic spin configuration, in particular at small doping.

For these reasons, we study in this chapter the system of spin $A_0^{\rm tr}$ and hole K interacting weakly through hopping $T_{\rm hop}$:

$$A \to A_0^{\rm tr}(z,\delta) + K(\psi,\eta) + T_{\rm hop}(z,\psi,\eta). \tag{3.25}$$

Before estimating the loop (or bubble) correction by $T_{\rm hop}$, we have to calculate the Green function of the hole fermion. They are evaluated as

$$\begin{aligned} <\psi_x(\tau)\overline{\psi}_{x'}(\tau')> &= \delta_{xx'}G_+(\tau,\tau') \\ <\eta_x(\tau)\overline{\eta}_{x'}(\tau')> &= \delta_{xx'}G_-(\tau,\tau') \equiv -\delta_{xx'}G_+(\tau',\tau), \end{aligned} \tag{3.26}$$

where,

$$G_+(\tau,\tau') = \frac{1}{1+e^{-\beta m}}(e^{-m(\tau-\tau')}\theta(\tau-\tau') - e^{-m(\beta+\tau-\tau')}\theta(\tau'-\tau)). \tag{3.27}$$

From eqs.(3.26)(3.27), we obtain a relation between δ and the hole mass m valid at $\delta \simeq 0$ as follows,

$$\delta \equiv <\overline{\psi}_x(\tau)\psi_x(\tau)> = \frac{e^{-\beta m}}{1+e^{-\beta m}} \simeq e^{-\beta m}. \tag{3.28}$$

Since the fermion mass (or chemical potential) m is chosen to satisfy the relation (3.28), the mass at fixed doping becomes smaller at lower temperature:

$$m \simeq -\frac{1}{\beta}\ln\delta. \tag{3.29}$$

The loop correction is now calculated as follows.

$$\begin{aligned} Z &\simeq \int [D\bar{z}zD\bar{\psi}\psi D\bar{\eta}\eta]\exp(-A_0^{\rm tr}(z) - K(\psi\eta) - T_{\rm hop}) \\ &= \int [D\bar{z}zD\bar{\psi}\psi D\bar{\eta}\eta]\left(1+\frac{1}{2}(T_{\rm hop})^2 + O(T_{\rm hop})^4\right)\exp(-A_0^{\rm tr}(z) - K(\psi\eta)) \\ &\simeq \int [D\bar{z}z]\exp(-A_0^{\rm tr})\exp\left[\frac{1}{2}\int d\tau\int d\tau'\sum_{oo'}\sum_{ij}t_it_j\right. \\ &\quad \left.\left(B_i(o\tau)C_j(o'\tau') < \bar{\psi}_{oi}(\tau)\bar{\eta}_o(\tau)\eta_{o'}(\tau')\psi_{o'j}(\tau') > + (oi\tau \rightleftharpoons o'j\tau')\right)\right. \\ &\quad \left. + O(T_{\rm hop})^4\right], \end{aligned} \tag{3.30}$$

where we have used

$$< \bar{\psi}\bar{\eta} > = < \eta\psi > = 0 \qquad \text{etc.} \tag{3.31}$$

We have taken only the one loop correction (Fig.3.5(a)). In the coordinate space, this is to include one site hoppings of holes (Fig.3.5(b)). The higher order hopping

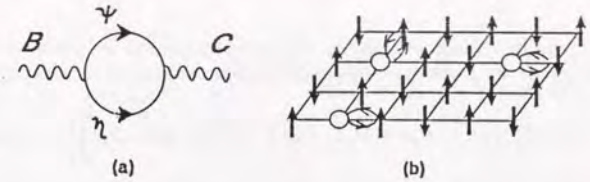

Figure 3.5: (a):One loop correction to the spin variable by the hole. (b):The same contribution in the coordinate space.

process are of $O(\delta^2)$ and neglected.

The expectation values are estimated using eq.(3.26) as

$$\begin{aligned} < \overline{\psi}_{oi}(\tau)\overline{\eta}_o(\tau)\eta_{o'}(\tau')\psi_{o'j}(\tau') > &= - < \overline{\psi}_o i(\tau)\psi'_o j(\tau') >< \eta_{o'}(\tau')\overline{\eta}_o(\tau) > \\ &\simeq \delta \times \delta_{oo'}\delta_{ij}. \end{aligned} \tag{3.32}$$

This quantity is $O(\delta)$, and does not depend on $\tau - \tau'$, since ψ and η propagate in the opposite directions in time. (see eq.(3.26)) Thus the one loop renormalization to $A_0^{\rm tr}$ is obtained as

$$\Delta A_0 \equiv -\delta\sum_o\sum_i t_i^2\int_0^\beta d\tau\int_0^\beta d\tau' B_i(o\tau)C_i(o\tau') \tag{3.33}$$

Our effective theory is from these considerations given by

$$A^{\rm eff} = A_0^{\rm tr} + \Delta A_0. \tag{3.34}$$

The term (3.33) is non local in the time direction. The non local interaction arises since the quantum fluctuation of the hole grows at low temperature, where the hole mass becomes small according to eq.(3.29). At sufficiently high temperature the range of integration $[0,\beta]$ is small and the expression may be replaced by a local form

$$\Delta A_0 \simeq -\delta\beta\sum_o\sum_i t_i^2\int_0^\beta d\tau B_i(o\tau)C_i(o\tau). \tag{3.35}$$

This localization is valid for small βJ, and so the resulting form diverges as $\beta \to \infty$. At very low temperature, therefore, the non locality of the loop correction must be taken into account seriously. There is a small factor δ in (3.35), and owing to this, the violent behavior at low temperature is somewhat suppressed. In the numerical calculation in Sect.3.5, the approximation (3.35) is seen to be valid at $T \gtrsim 100$K.

Let us now take the continuum limit of the effective action obtained above by assuming smoothness of the field. The continuum limit of $A_0^{\rm tr}$, up to $O(D^2)$ is the following anisotropic CP^1 σ-model,

$$A_0^{\rm tr}(\delta) \to A_{CP^1}^0(\delta)$$

$$\equiv \frac{J}{2a_3}\int_0^\beta d\tau \int d^3x \left[\frac{1}{(2+\alpha)J^2a^2}\overline{D_\tau z}\cdot D_\tau z + (1-\delta)^2\left\{\overline{D_x z}\cdot D_x z + \overline{D_y z}\cdot D_y z + \alpha\left(\frac{a_3}{a}\right)^2 \overline{D_z z}\cdot D_z z\right\}\right], \quad (3.36)$$

with the constraint $\bar{z}\cdot z = 1$. In eq.(3.36), the covariant derivatives are, $D_\tau z = (\partial_\tau - \bar{z}\cdot\dot{z})z, D_\mu z = (\partial_\mu - \bar{z}\cdot\partial_\mu z)z$. In the above action, all the parameters in the low energy effective field theory are determined by microscopic parameters a, a_3, J and α.

The one loop correction ΔA_0 also reduces to the similar form ΔA_{CP^1} in the continuum limit.

$$\Delta A_{CP^1} \equiv -\frac{\delta\beta t^2}{a_3}\int_0^\beta d\tau\int d^3x\left\{\overline{D_x z}\cdot D_x z + \overline{D_y z}\cdot D_y z + \alpha\left(\frac{a}{a_3}\right)^2\overline{D_z z}\cdot D_z z - \frac{1}{2J^2a^2}\overline{D_\tau z}\cdot D_\tau z\right\}. \quad (3.37)$$

In all, we have the following action up to order δ as an effective field theory of the magnetic part of the t-J model,

$$\begin{aligned} A_{CP^1} &\equiv A^0_{CP^1} + \Delta A_{CP^1} \\ &= \frac{J_{\rm eff}}{2a_3}\int d\tau\int dx^3\left[\frac{\left(1+2\delta+\frac{2t^2\beta\delta}{J}(2+\alpha)\right)}{(2+\alpha)J^2a^2}\overline{D_\tau z}\cdot D_\tau z\right. \\ &\left. + (\overline{D_x z}\cdot D_x z + \overline{D_y z}\cdot D_y z) + \alpha\left(\frac{a_3}{a}\right)^2\overline{D_z z}\cdot D_z z\right], \end{aligned} \quad (3.38)$$

where

$$J_{\rm eff} \equiv J\left(1 - 2\delta - \frac{2t^2\beta\delta}{J}\frac{2+\alpha}{2}\right). \quad (3.39)$$

This effective antiferromagnetic coupling $J_{\rm eff}$ diminishes as doping increases. In the following sections, we will investigate the phase diagram of this CP^1 model. We will find that there are, as expected, two phases; one is the ordered phase with long range antiferromagnetic order, and the other is the disordered phase with the mass gap in the spin excitation.

3.3 Saddle point approximation of the CP^1 model

As discussed in the previous section, the effective action appropriate to describe slightly doped high T_c materials is an anisotropic CP^1 σ model in (3+1)-dimensions. By restoring $\hbar$, Its action eq.(3.38) is explicitly written as

$$\frac{1}{\hbar}A_{CP^1} = \frac{1}{g(\delta)}\int_0^\beta d\tau\int d^3x\left[|D_x z|^2 + |D_y z|^2 + \alpha\lambda|D_z z|^2 + \frac{1}{(\hbar c(\delta))^2}|D_\tau z|^2\right], \quad (3.40)$$

with α stand for the weakness of the antiferromagnetic coupling in the z-direction, and λ is the anisotropy parameter of the lattice:

$$\begin{aligned} \alpha &= J_z/J \\ \lambda &= (\frac{a_3}{a})^2. \end{aligned} \quad (3.41)$$

The effects of holes are contained in the doping dependence of the coupling constant $g(\delta)$ and the spin velocity $c(\delta)$:

$$\begin{aligned} g(\delta) &= \frac{2a_3}{J}\left[1 + 2\delta + \frac{2t^2\beta\delta}{J}\frac{2+\alpha}{2}\right] \\ \hbar c(\delta) &= \sqrt{2+\alpha}Ja\left[1 - \delta - \frac{2t^2\beta\delta}{J}\frac{2+\alpha}{2}\right]. \end{aligned} \quad (3.42)$$

Rescaling the imaginary time τ by $\hbar c$, we get the usual form of CP^1 model

$$\frac{1}{\hbar}A_{CP^1} = \frac{1}{f}\int_0^{\beta\hbar c} d\tau\int d^3x\left[|D_x z|^2 + |D_y z|^2 + \alpha\lambda|D_z z|^2 + |D_\tau z|^2\right], \quad (3.43)$$

where $f(\delta) \equiv g(\delta)\hbar c(\delta)$ is an effective σ-model coupling constant.

Note that there is no ultra violet divergence, since the space integral has cutoff at lattice spacing a and a_3. In the momentum space, this leads to the following integration range with ultra violet cutoffs:

$$\begin{aligned} 0 &\lesssim k_1, k_2 \lesssim \Lambda \\ 0 &\lesssim k_3 \lesssim \Lambda_3, \end{aligned} \quad (3.44)$$

where

$$\begin{aligned} \Lambda &\equiv \frac{\sqrt{2\pi}}{a} \\ \Lambda_3 &\equiv \frac{\pi}{a_3}. \end{aligned} \quad (3.45)$$

The cutoff Λ is so chosen as to preserve the area of half the Brillioun zone in the $X-Y$ plane. Remember that the field z here represents the spins on the even site of the original lattice.

The dimensionless coupling constant $\hat{f}$ is defined as

$$\begin{aligned} \hat{f}(\delta) &\equiv f(\delta)\Lambda^2 \\ &= 4\pi\sqrt{2+\alpha}\sqrt{\lambda}(1+\delta). \end{aligned} \quad (3.46)$$

The one loop contribution cancels out in $\hat{f}$.

We can check that this $\hat{f}$ at $\delta = 0$ is surely in the weak coupling region. Explicitly, the critical coupling of the CP^1 model with weak three-dimensionality

is give by $\hat{f}_c^{(CP1)} \equiv 4\sqrt{2\lambda\pi^3}$. If $\hat{f}$ is above this value, quantum fluctuations of spins are large enough to destroy the antiferromagnetic order even at zero temperature. Our $\hat{f}(\delta = 0, \alpha \simeq 0)$ is smaller than $\hat{f}_c$ by a factor $\sqrt{\pi}^{-1} = 0.56$. This fact show that the t-J model is a good starting point to study real high T_c materials (since they do have antiferromagnetic ordered phase). The action eq.(3.40) has an alternative representation, i.e., $O(3)$ nonlinear σ model. The $O(3)$ variable is the three component real vector $\vec{\varphi} = \varphi_i (i = 1 \sim 3)$:

$$\varphi_i(x) \equiv \sum_{\sigma\sigma'} \bar{z}_{x\sigma} \sigma^i_{\sigma\sigma'} z_{x\sigma'}, \tag{3.47}$$

with σ^i = Pauli matrices. Because of the CP^1 constraint (3.6), the field $\vec{\varphi}$ is of unit length:

$$\vec{\varphi}^2(x) = 1. \tag{3.48}$$

In terms of this $O(3)$ variable, the action (3.40) is written as

$$\frac{1}{\hbar} A_{O(3)} = -\frac{1}{4f} \int_0^{\beta\hbar c} d\tau \int d^3x [\sum_{j=x,y,\tau} (\partial_j \vec{\varphi})^2 + \alpha\lambda (\partial_z \vec{\varphi})^2]. \tag{3.49}$$

We used the relation $|D_x z|^2 = (\partial_x \vec{\varphi})^2/4$ etc. Correspondingly, the measure is transcribed as $d\bar{z}dz\delta(\bar{z}z - 1) = d\vec{\varphi}\delta(\vec{\varphi}^2 - 1)$. For calculations of magnetization and susceptibility this O(3) representation is more convenient than the CP^1 representation. This is because, if we adopt the latter, we have to deal with the composite operators of CP^1 variables in such calculations.

We expect that our field-theory model gives a good description of the long-range behavior of the spin dynamics of doped high T_c materials. Here the parameters are the antiferromagnetic Heisenberg exchange coupling J and the anisotropic parameter α. They shall be determined in Sect.3.5 by the comparison of theoretical results with the experiments on La_2CuO_4. For the lattice spacings a, a_3 (hence also for $\lambda = (a_3/a)^2$), definite values will be used there throughout the analysis.

In the following, being based on the above anisotropic $O(3)$ model (3.49), we will perform the field theoretical calculation of the effective potential for the antiferromagnetic order parameter (the third component of the spin variable $\vec{\varphi}$) and the auxiliary field σ (spin mass gap) introduced to keep the constraint $\vec{\varphi}^2 = 1$, and derive its saddle point equations[37,38]. This procedure is equivalent to the derivation of the mean field equations for these order parameters. The saddle point (or mean field) approximation makes sense here, since we are working on the (weakly) three-dimensional case.

We write the partition function of this system as a Euclidean path-integral

$$\begin{aligned} Z(\beta) &= \int D\varphi_1 D\varphi_2 D\varphi_3 D\sigma \exp\left(-\frac{1}{\hbar}\hat{A}_{O(3)}\right), \\ \frac{1}{\hbar}\hat{A}_{O(3)} &= \frac{1}{2}\int_0^{\beta\hbar c} d\tau \int d^3x \left[\sum_{j=x,y,\tau} (\partial_j \vec{\varphi})^2 + \alpha\lambda(\partial_z\vec{\varphi})^2 + \sigma(\vec{\varphi}^2 - \frac{1}{2f})\right], \end{aligned} \tag{3.50}$$

where the replacement $\vec{\varphi} \to \sqrt{2f}\vec{\varphi}$ has been made. Integrating out φ_1 and φ_2 we obtain an effective action of φ_3 and σ fields

$$Z(\beta) = \int D\varphi_3 D\sigma \exp\left[-\frac{1}{2}\int_0^{\beta\hbar c} d\tau \int d^3x \left\{\sum_{j=x,y,\tau} (\partial_j\varphi_3)^2 + \alpha\lambda(\partial_z\varphi_3)^2 + \sigma(\varphi_3^2 - \frac{1}{2f})\right\} - \mathrm{Tr}\ln\left(\sum_{j=x,y,\tau}\partial_j^2 + \alpha\lambda\partial_z^2 + \sigma\right)\right]. \tag{3.51}$$

This Tr ln term is calculated by Fourier transform:

$$\begin{aligned} &\mathrm{Tr}\ln\left(\sum_{j=x,y,\tau}\partial_j^2 + \alpha\lambda\partial_z^2 + \sigma\right) \\ &= \int d^{3+1}x \frac{1}{\beta\hbar c}\sum_{\ell=-\infty}^{\infty}\int^{\Lambda,\Lambda_3}\frac{d^3\mathbf{k}}{(2\pi)^3}\ln\left(1 + \frac{\sigma}{k_1^2 + k_2^2 + \alpha\lambda k_3^2 + \omega_\ell^2}\right), \end{aligned} \tag{3.52}$$

with $\omega_\ell = 2\pi\ell/\beta\hbar c$ (ℓ:integer).

Thus, up to the constant, we get an effective potential V_{eff} (defined through $S_{eff} = \int d^{3+1}x V_{eff}$) for φ_{3_c} (the antiferromagnetic order parameter) and σ_c (the spin mass gap) where the subscript c means the constant configuration,

$$\begin{aligned} V_{eff}(\varphi_{3_c}, \sigma_c) &= \frac{1}{2}\sigma_c\left(\varphi_{3_c}^2 - \frac{1}{2f}\right) \\ &+ \frac{1}{\beta\hbar c}\sum_{\ell=-\infty}^{\infty}\int\frac{d^3\mathbf{k}}{(2\pi)^3}\ln\left(1 + \frac{\sigma_c}{k_1^2 + k_2^2 + \alpha\lambda k_3^2 + \omega_\ell^2}\right). \end{aligned} \tag{3.53}$$

From this, saddle point conditions for σ_c and φ_{3_c} follow easily

$$\begin{aligned} 0 &= \frac{\partial V_{eff}}{\partial\sigma_c} \\ &= \frac{1}{2}\left(\varphi_{3_c}^2 - \frac{1}{2f}\right) + \frac{1}{\beta\hbar c}\sum_{\ell=-\infty}^{\infty}\int\frac{d^3\mathbf{k}}{(2\pi)^3}\frac{1}{\omega_\ell^2 + k_1^2 + k_2^2 + \alpha\lambda k_3^2 + \sigma_c}, \end{aligned} \tag{3.54}$$

$$0 = \frac{\partial V_{eff}}{\partial\varphi_{3_c}} = \sigma_c\varphi_{3_c}. \tag{3.55}$$

Using the method of the complex integral, the second term on the right hand side of (3.54) ($\equiv I$) can be rewritten as

$$I = \int\frac{d^3\mathbf{k}}{(2\pi)^3}\frac{1}{2\omega}\coth\left(\frac{\beta\hbar c\omega}{2}\right), \tag{3.56}$$

where $\omega^2 = k_1^2 + k_2^2 + \alpha\lambda k_3^2 + \sigma_c$. In Sect.3.5, evaluating this integral numerically, we investigate in detail the solutions of saddle point equations (3.54) and (3.55) which describe the various magnetic properties of high T_c materials.

Let us explain how physical quantities are obtained from the saddle point conditions. The equation (3.55) implies that there may be two phases, namely, $\sigma_c = 0$ and $\varphi_{3_c} = 0$. The quantity σ_c is the mass of the φ-field so that the correlation length ξ of the spins are given as $\xi = \sqrt{\sigma_c}^{-1}$. Thus, in the phase $\sigma_c = 0$, the spins are Néel ordered($\xi = \infty$). As shown in [39], where the CP^1 sigma model is considered, the ordered phase exists at sufficiently low temperature, and in this phase, φ_{3_c} calculated from eq.(3.54) with $\sigma_c = 0$ is non-vanishing. φ_{3_c} is related to the staggered magnetization $M(x) \equiv 2(-)^x < S_z(x) >$ as $M = \sqrt{2f}\varphi_{3_c}$, since the φ-field is normalized as $\vec{\varphi}^2 = 1/(2f)$ in eq.(3.54). M is normalized to be unity when the system is saturated to the complete antiferromagnetic order. The staggered magnetization decreases as the temperature increases, and vanishes at some temperature. This temperature, the Néel temperature T_N, is determined by eq.(3.54) with both σ_c and φ_{3_c} set to zero. The region $T > T_N$ is the disordered phase, where $\varphi_{3_c} = 0$ and $\sigma_c \neq 0$. In this phase, the inverse correlation length $\sqrt{\sigma_c}$ is obtained from eq.(3.54) by setting $\varphi_{3_c} = 0$.

Before that, in the next section, we will see the asymptotic ($\alpha \to 0$) behavior of the solutions.

3.4 $\alpha \to 0$ limit of the solution at zero doping

In the following three sections, we study the behaviors of the physical quantities such as Néel temperature T_N and the spin correlation length ξ as the solutions of the saddle point equations (3.54) and (3.55). First, we consider in this section only their asymptotic ($\alpha \to 0$ or $J_3 \to 0$) behaviors. For general value of α, the equations cannot be solved analytically and numerical calculations are necessary(see Sect.3.5).

The study of this asymptotic behavior itself is of academic interest. At $\alpha = 0$, the system is exactly two-dimensional. There may appear crossover phenomena from three-dimensions to two-dimensions at some value of α, $\alpha_{c.o.}$, or at some characteristic length with fixed α. For example, for the classical XY model, the critical temperature is obtained as a function of $\alpha(<< 1)$ by the scaling argument[40],

$$T_c(\alpha) = T_{\rm KT} + \frac{a}{(\ln \alpha)^2}, \tag{3.57}$$

where $T_{\rm KT}$ is the Kosterlitz-Thouless transition temperature and a is some constant. The crossover phenomena are also studied by Monte Carlo simulations[41].

Now we analyze equations. The integral I in eq.(3.56) is written after performing the k_1, k_2-integral as

$$I = \frac{\Lambda^2 u}{2\hat{f}_c}\int_0^1 dx \left(\ln\sinh \frac{\sqrt{1+\frac{\pi}{2}\alpha x^2 + \tilde{\sigma}}}{2u} - \ln\sinh \frac{\sqrt{\frac{\pi}{2}\alpha x^2 + \tilde{\sigma}}}{2u} \right), \tag{3.58}$$

where

$$x = \frac{k_3}{\Lambda_3}, \qquad \hat{f}_c = \sqrt{2\lambda\pi^3}, \qquad u = \frac{1}{\beta\hbar c\Lambda}, \qquad \tilde{\sigma} = \frac{\sigma_c}{\Lambda^2}. \tag{3.59}$$

$\hat{f}_c$ is the two-dimensional critical coupling (see e.g., eq.(3.62))[1].

The saddle point condition (3.54) then becomes

$$2\tilde{\varphi}_3^2 = \frac{1}{\hat{f}} - \frac{2u}{\hat{f}_c}\int_0^1 dx \left(\ln\sinh \frac{\sqrt{1+\frac{\pi}{2}\alpha x^2 + \tilde{\sigma}}}{2u} - \ln\sinh \frac{\sqrt{\frac{\pi}{2}\alpha x^2 + \tilde{\sigma}}}{2u} \right), \tag{3.60}$$

where $\tilde{\varphi}_3 \equiv \varphi_{3_c}/\Lambda$ is the dimensionless antiferromagnetic order parameter. From eq.(3.60) we see that, in the disordered phase ($\tilde{\varphi}_3 = 0$), if $\tilde{\sigma} \gg \alpha$, i.e., in temperature sufficiently higher than T_N, the coupling in the third direction(represented by α) can be neglected and the system shows two-dimensional($\alpha = 0$) behavior. On the other hand, very close to the Néel temperature(i.e. $\tilde{\sigma} \ll \alpha$), the behavior of $\tilde{\sigma}$ will differ from the two-dimensional one. Below we assume $\alpha \ll 1$ and study the above two cases separately.

Let us first see the $\tilde{\sigma} \gg \alpha$ case. Expanding the integral I in terms of α, the saddle point condition (3.60) with $\tilde{\varphi}_3 = 0$ is shown to be

$$\begin{aligned} 0 = &\frac{1}{2u}\frac{\hat{f}_c}{\hat{f}} - \ln\sinh\frac{\sqrt{1+\tilde{\sigma}}}{2u} + \ln\sinh\frac{\sqrt{\tilde{\sigma}}}{2u} \\ &-\frac{\pi\alpha}{24u}\left(\frac{\coth\frac{1+\tilde{\sigma}}{2u}}{\sqrt{1+\tilde{\sigma}}} - \frac{\coth\frac{\tilde{\sigma}}{2u}}{\sqrt{\tilde{\sigma}}} \right) + O(\alpha^2). \end{aligned} \tag{3.61}$$

The terms containing α on the right hand side represent the difference between the three- and two-dimensional systems. This difference becomes smaller as $\tilde{\sigma}$ grows. When ($\alpha \ll$)$\tilde{\sigma} \ll 1$, eq.(3.61) is reduced to a simple form:

$$\sqrt{\sigma_c} \simeq \frac{k_B T}{\hbar c}\exp\left(-\frac{\hbar c\Lambda}{2k_B T}\left(\frac{\hat{f}_c}{\hat{f}} - 1\right)\right). \tag{3.62}$$

This is the same as those obtained in [30,39,42]

The three-dimensional effect becomes important when $\tilde{\sigma} \ll \alpha$. Expanding I by α and $\tilde{\sigma}/\alpha$, we get

$$I = \frac{u\Lambda^2}{2\hat{f}_c}\left(\ln(2u\sinh\frac{1}{2u}) - \frac{1}{2}\ln\frac{\pi}{2}\alpha + 1 - \sqrt{\frac{\pi\tilde{\sigma}}{2\alpha}} + O(\alpha, \frac{\tilde{\sigma}}{\alpha}) \right). \tag{3.63}$$

Since we are considering the asymptotic limit $\alpha \ll 1$, we can use the fact that u is small: $u \ll 1$. This inequality holds because $\alpha \ll 1$ means $T_N \approx 0$ and we are interested in the region $T \simeq T_N$. The realistic value of $\hbar c\Lambda$ for La_2CuO_4 (with $a = 3.8\mathring{A}$) is $\hbar c\Lambda \simeq 5000$K, so that T less than the room temperature is sufficient to satisfy $u \ll 1$. Then the saddle point equation (3.60) can be approximated as

$$2\tilde{\varphi}_3^2 \simeq \left(\frac{1}{\hat{f}} - \frac{1}{\hat{f}_c}\right) - \frac{u}{\hat{f}_c}\left(-\ln\frac{\pi}{2}\alpha + 2\ln u + 2 - \sqrt{\frac{2\pi\tilde{\sigma}}{\alpha}} \right). \tag{3.64}$$

[1] The critical coupling $\hat{f}_c^{(CP1)}$ for the CP1 model (appeared below eq.(3.46)) is four times that for the O(3) model $\hat{f}_c$, owing to the identity $|D_\mu z|^2 = (\partial_\mu \vec{\varphi})^2/4$.

We can obtain T_N from this equation by setting $\tilde{\varphi}_3 = \tilde{\sigma} = 0$. When α is small enough to satisfy the condition $\alpha/u^2 \ll 1$, picking only the $-\ln\alpha$ term in the second bracket on the right hand side of eq.(3.64), we get an asymptotic expression for T_N:

$$k_B T_N \simeq \frac{\hbar c \Lambda (\frac{\hat{f}_c}{\hat{f}} - 1)}{-\ln \alpha}. \tag{3.65}$$

This expression can be obtained also in the one loop renormalization group analysis[35]. The Néel temperature goes to zero slowly as $\alpha \to 0$. Since the ratio α/T_N^2 is $O(\alpha(\ln\alpha)^2)$, the condition $\alpha/u^2 \ll 1$ holds if α is sufficiently small and if $T \approx T_N$. More explicitly, noting that eq.(3.65) is obtained by neglecting $O(2\ln|\ln\alpha|/\ln\alpha)$-terms we find eq.(3.65) to be approximately valid within, for example, about 10 percent error, if

$$\alpha \lesssim 10^{-40}. \tag{3.66}$$

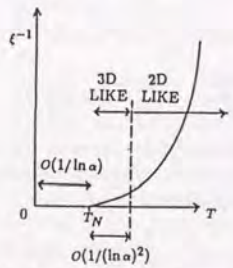

Figure 3.6: The schematic behavior of inverse correlation length near the critical point when $\alpha \ll 1$

The staggered magnetization φ_{3_c} and the inverse correlation length $\sqrt{\sigma_c}$ are obtained as functions of $(T - T_N)$ by taking the difference between eq.(3.64) with $T = T_N$ and that with an arbitrary T. Up to the lowest order in $(T - T_N)$, the equation thus obtained is

$$2\hat{f}_c \tilde{\varphi}_3^2 \simeq (u - u_N)\left(\ln\frac{\pi}{2}\alpha - 2\ln u_N - 2\right) + u\sqrt{\frac{2\pi\tilde{\sigma}}{\alpha}}, \tag{3.67}$$

where $u_N \equiv k_B T_N/\hbar c\Lambda$.

Under the same condition as eq.(3.66), we obtain from eq.(3.67)

$$M \simeq \sqrt{(-\ln\alpha)\frac{\hat{f}}{\hat{f}_c}\frac{k_B}{\hbar c\Lambda}(T_N - T)}, \tag{3.68}$$

$$\sqrt{\sigma_c} \simeq \frac{\Lambda}{\pi}\sqrt{\frac{\pi}{2}\alpha}(-\ln\alpha)\frac{T - T_N}{T_N}. \tag{3.69}$$

near the critical temperature. As seen from eq.(3.68) we find the critical exponent of the staggered magnetization is 1/2 in mean field theory. The inverse correlation length rises linearly starting at the Néel temperature. The critical exponent -1 is that of the classical(i.e. $T = \infty$) three-dimensional(isotropic) $O(3)\sigma$ model at the one-loop order[43] Therefore, at least at one-loop level, the quasi-two-dimensional spin system has a three-dimensional behavior in the region very close to the critical point even though the coupling in the third direction is very weak. This is quite natural. Since the correlation length is very large near the critical point, the spins feel the effects of the third direction no matter how weak the coupling is. The three-dimensional effects become negligible when $\tilde{\sigma}$ exceeds α, as seen from eq.(3.60). Using eq.(3.69), the region of three-dimensional behavior ($\tilde{\sigma} \lesssim \alpha$) is shown to be $(T - T_N) \lesssim O(\ln\alpha)^{-2}$. (See Fig.3.6.) This region is too narrow to be seen clearly by experiments, and this explains why the two-dimensional analysis[30] can reproduce the experimental results on correlation length globally.

3.5 Numerical solutions at zero doping

In the previous section, the asymptotic($\alpha \to 0$) behaviors of the solutions of the saddle point conditions(3.54) and (3.55) were investigated. In this section, we will study the solutions for realistic values of $\alpha(\approx 10^{-5})$ with the help of numerical calculations, and investigate the magnetic properties of La_2CuO_4 in detail.

As explained in Sect.3.3, from the saddle point conditions we can calculate the magnetic quantities such as the Néel temperature, the correlation length and the staggered magnetization of pure and doped La_2CuO_4. The correlation length was previously calculated in [30] by using a different approach in the framework of the two-dimensional σ-model, and we will show that our results are consistent with theirs.

In this paper we will take $a = 3.8$Å, the shortest Cu-Cu distance in the Cu-O planes and $a_3 = 6.6$Å, the distance between the planes, hence $\lambda = 3.0$. We have verified that the physical quantities like T_N, ξ/a and M are not sensitive to the cutoff parameter, the lattice spacings. The three parameters in our model; $\hat{f}$ [2] , J(which is related to $\hbar c$ by eq. (3.42)) and α are determined by comparing our numerical results with the experimental data on pure La_2CuO_4. The neutron scattering experiment has been done on La_2CuO_4 by [36] Their best sample has the antiferromagnetic long-range order up to $T_N = 195$K. The spin correlation length and the staggered magnetization were also observed for this sample.

As we will see later, the Néel temperature and the correlation length at $\delta = 0$ are sufficient to fix the three parameters. We can then use these parameters to predict the staggered magnetization. The T_N-δ phase diagram is also calculated with the additional input parameter t. Furthermore, the parameters determined

[2] In our derivation in Sect.3.1, $\hat{f}$ at $\delta = 0$ is determined. However, in the derivation, we have neglected finite renormalization due to higher derivative terms, and it may be better to treat $\hat{f}$ as a free parameter and fix its value from the comparison with experiments.

will be shown to be in good agreement with previous estimates obtained by other methods.

In the following calculations, we will first set the σ model coupling constant $\hat{f}$ to be $\hat{f} = 0.69\hat{f}_c$($\hat{f}_c$ is the two-dimensional critical coupling and is given by eq.(3.59)). This value is the same as that claimed to give good fits to the experiments[36] in two-dimensional σ model analysis[30]. Also in our calculation, other choices of $\hat{f}$ cannot reproduce the experimental results of T_N and ξ(see below).

Let us show the numerical results.

Néel temperature We first observe how the Néel temperature depends on two parameters J (which is related to $\hbar c$ by eq.(3.42)) and α. The dependence of T_N on α with J being fixed is shown in Fig.3.7. When α is zero, the Néel temperature is zero, as expected from the Mermin-Wagner theorem[31]. As α increases, the effect of the third dimension becomes larger and T_N increases. As easily seen in these figures, α must be very small($\approx 10^{-7} \sim 10^{-5}$) in order to obtain $T_N \simeq 195$K, which is smaller by factor ≈ 5 compared with J of about 0.1eV($\sim$ 1000K). Note that the approximation used in Sect.3.4 is valid only for much smaller α. On the other

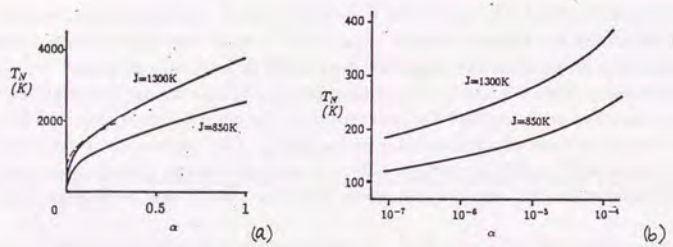

Figure 3.7: (a):T_N-α diagram with fixed J. Solid lines are numerical results for $J = 850$K and $J = 1300$K. The dotted line is the result with $J = 850$K of an approximate equation valid for not small α. $\hat{f}$ is $0.69\hat{f}_c$ (b):The small α region.

hand, T_N increases together with J (or $\hbar c$) for fixed α, because the temperature and $\hbar c$ appear in equation (3.54) in a form of $\beta\hbar c$.

Spin correlation length Fig.3.8 shows our fits to the results of experiments [36] on La_2CuO_4. The Néel temperature of this sample is 195K. The best fit (solid line) is obtained for $\alpha = 1.7 \times 10^{-5}$ and $\hbar c = 0.39$eVÅ. This value of $\hbar c$ is essentially the same as that obtained in [30] using the one-loop renormalization-group approach. Smaller and larger $\hbar c$ cannot reproduce the experimental result. For example, $\hbar c = 0.60$eVÅ(α is 2.0×10^{-7} for $T_N = 195$K) gives much smaller ξ^{-1}(dotted line). The above value of $\hbar c$ corresponds to $J = 0.073$eV, as seen from eq.(3.42)). This value is of the same order ($\simeq 10^3$K) as obtained in Raman

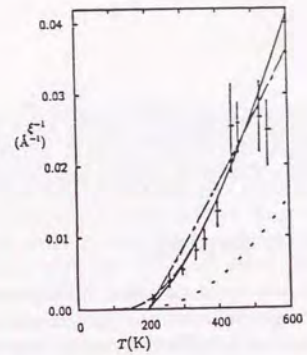

Figure 3.8: The inverse correlation length ξ^{-1} versus temperature. Using $\hat{f} = 0.69\hat{f}_c$ with T_N fixed at 195K, the best fit(solid line) is obtained for $\hbar c = 0.39$eVÅ and $\alpha = 1.7 \times 10^{-5}$. The result with $\hbar c = 0.60$eVÅ is shown by a dotted line. Dashed line is the result with $\alpha = 0$ ($\hbar c = 0.39$eVÅ) using the same $\hat{f}$. Dotted-dashed line is the best fit using $\hat{f} = 0.89\hat{f}_c$ with T_N fixed at 195K ($\hbar c$ is 0.75eVÅ). The experimental data are taken from [36].

scattering experiment[44]. The value of α we found is also in good agreement with the result of the previous analysis[45].

Let us check that our calculation contains the results of two-dimensional analysis in [30] by setting $\alpha = 0$. Chakravarty et al. obtained the correlation length by the renormalization group approach, and we directly calculated the mass of the φ-field which is dynamically generated. These two results are essentially the same. The correlation length with $\alpha = 0$ (dashed line) differs from the result with $\alpha = 1.7 \times 10^{-5}$ only for T smaller than 300K. For the range of temperature larger than 300K, these two almost coincide, as mentioned in Sect.3.4.

It should also be pointed out that smallness of α means very short correlation length in the third direction, as seen in the following way. The spin-spin correlation function is

$$< \vec{\varphi}(\vec{x})\vec{\varphi}(0) > \simeq \sum_t \int d^3k \frac{e^{i\vec{k}\cdot\vec{x}}}{k_1^2 + k_2^2 + \alpha\lambda k_3^2 + \omega_t^2 + \sigma_c}$$
$$\propto \sum_t \int d^2k d\tilde{k}_3 \frac{e^{ik_1x_1 + ik_2x_2 + i(\alpha\lambda)^{-\frac{1}{2}}\tilde{k}_3x_3}}{k_1^2 + k_2^2 + \tilde{k}_3^2 + \omega_t^2 + \sigma_c}, \qquad (3.70)$$

where $\tilde{k}_3 = \sqrt{\alpha\lambda}k_3$. From this expression, it is seen that for $\vec{x}$ lying in the X-Y plane,

$$< \vec{\varphi}(\vec{x})\vec{\varphi}(0) > \to \exp(-\sqrt{\sigma_c}|\vec{x}|), \qquad (3.71)$$

as $|\vec{x}| \to \infty$, while for $\vec{x}$ pointing in the third direction,

$$< \vec{\varphi}(\vec{x})\vec{\varphi}(0) > \to \exp(-\frac{\sqrt{\sigma_c}}{\sqrt{\alpha\lambda}}|\vec{x}|). \qquad (3.72)$$

That is, the interlayer correlation length ξ_3 is smaller than the correlation length in the CuO-plane by the factor of $\sqrt{\alpha\lambda} \approx 0.7 \times 10^{-2}$. Actually, the experiment shows that ξ_3 is about 2Å while $\xi \approx 200$Å at room temperature[36].

3.6 Solutions at finite doping

Néel temperature Now we consider the doped case. As explained in Sect.3.1, the presence of holes disturbs the magnetic order, and T_N decreases as δ increases. If we ignore the hole hopping, i.e. at the tree (Hartree) level of the hole dynamics, the coupling constant and the spin-wave velocity are renormalized as $1/f \to (1-\delta)^2/f$ and $\hbar c \to \sqrt{2+\alpha}(1-\delta)Ja$, respectively (removing the one loop correction ($\propto \beta\delta$) from eqs. (3.42) and (3.46)). By substituting the above to the saddle point equations (3.54) and (3.55), we calculate T_N at the tree level as a function of δ. This tree level result of the T_N-δ phase diagram is shown in Fig.3.9 with the dashed line. The Néel temperature T_N decreases proportionally to the hole density, and vanishes at $\delta \approx 0.32$. That is, there is no long range Néel order for $\delta > 0.32$. However, in the experiments, the Néel order disappears at about 0.03. This fact shows that the hole hopping gives quite important effects to the spin dynamics. In order to estimate these effects, we have calculated the contribution

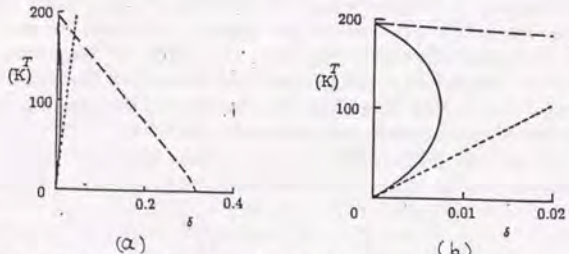

Figure 3.9: (a):T_N-δ phase diagram. $\hat{f} = 0.69\hat{f}_c$, $\hbar c = 0.39\text{eV}\text{Å}$, $\alpha = 1.7 \times 10^{-5}$, $t = 0.13eV$. The lower region is the Néel ordered region. Dashed and solid line is the result at the tree and one-loop level of the hole dynamics, respectively. The importance of the hole hopping in decreasing T_N is clearly seen. Below the dotted line, the short range spiral state is realized, and the band motion of the hole starts. (b):The same in small δ region.

from T_{hop} at the one-loop (quantum) level in Sect.3.1, and the result is nonlocal in the time direction (without any damping factor) eq.(3.33). This nonlocality can be negligible at high temperature since the interval of τ-integration shrinks and eq.(3.35) was obtained. It may be a reasonable simplification down to the moderate value of temperature as discussed below. Then the one-loop effect, together with the tree-level renormalization, results in the renormalizations of $\hat{f}$

and $\hbar c$ as shown in eqs.(3.42) and (3.46). Using a typical value of $t \sim 0.13$eV (which corresponds to the typical magnitude of Coulomb repulsion energy of $U \sim 1$eV, since we have estimated $J = 4t^2/U = 0.073$eV from the study of correlation length.), we obtain the T_N-δ line (although this value of t is small compared to that obtained experimentally:$\simeq 0.4 \sim 0.5$eV). As a result, the Néel temperature decreases much more rapidly than the increase of the hole density (solid lines in Fig.3.9). Compared with the tree-level result, the value of δ at fixed T_N is now reduced by factor ≈ 30. However, this calculation becomes not reliable in low-temperature region. In fact, below 100K, the solution of the saddle point equation gives rise to a T_N-δ curve which bends into smaller δ side for lower temperatures, even though the renormalization factor $2t^2\beta\delta/J$ is still small at that point $(2t^2\beta\delta/J)_{T_N=100K} \sim 0.3$. From the behavior above 100K, it may be said that T_N vanishes at $\delta \sim 0.02$. But we conclude here only that static holes cannot destroy the order at $\delta \sim 0.03$, and the hole hopping is essential to disorder the system.

As a test, we have also investigated the two-loop renormalization effect, and found that it has an opposite sign to the one-loop renormalization, and it slightly improves $T_N - \delta$ line. Anyway, the re-entrant behavior of $T_N - \delta$ line is due to the localization of the nonlocal term (3.33). Hence, in order to get a $T_N - \delta$ line which may give a better fit with the experiments, it is necessary to treat this nonlocal term more properly. This problem is under study.

3.7 Short range spiral state

Next, let us discuss the (short range) spiral state[26] in our approach based on the effective action on lattice (3.34) in two dimensions. The one-loop correction by the hole is taken into account in the high temperature approximation (eq.(3.35)). The four fermi terms are neglected here. As δ increases further outside the $T_N - \delta$ line, the renormalized antiferromagnetic coupling J becomes even smaller and changes its sign at $\delta_c^{(sp)} \equiv J/2(J+\beta t^2)$(see eq.(3.38)). Beyond this $\delta_c^{(sp)}$, the system is no longer described by the renormalized CP^1 model. A new configuration of $z(x)$, the (short range) spiral state, is favored (see Fig.4.1). This can be understood within the mean field theory in the following way. Let us assume that in the x-y plane, the spin is rotated by an angle $2Q_x(2Q_y)$ as its coordinate increases by a in the positive x(y)-direction. The angle Q_μ is $O(\delta)$ and the nonvanishing Q_μ's indicates the spiral order. The above configuration is parametrized by $\tilde{V}_1 = 0, \tilde{V}_2 = \sin(Q_x - Q_y), \tilde{V}_3 = \sin(2Q_x), \tilde{V}_4 = \sin(Q_x + Q_y)$, where $\tilde{V}_i \equiv \bar{\xi}_\epsilon z_{o\epsilon}$. The (1,1)-spiral state [22] corresponds to $Q_x = Q_y (\equiv Q)$. We expand the action in terms of Q up to $O(Q^4)$. The variables $\bar{z}_\epsilon z_{o\epsilon}$'s are $1 + O(Q^2)$ for small Q in the above parametrization. For this choice, the lattice effective action for the spin variable including the one-loop correction (eq.(3.35)) is written as

$$S^{eff}(Q) = \beta \sum_o \left[2J \left(1 - 2\delta - \frac{2t^2\beta\delta}{J} \right) Q^2 \right.$$

$$+\frac{16J}{3}\left(1-2\delta-\frac{t^2\beta\delta}{2J}\right)Q^4+O(Q^6)\Big]. \qquad (3.73)$$

From this expression, it is seen that, the mean field value of Q is zero for $\delta < \delta_c^{(sp)}$, while Q becomes nonvanishing for $\delta > \delta_c^{(sp)}$: namely, the (short range) spiral state is realized (Fig.3.10). This state is the result of the ferromagnetic interaction

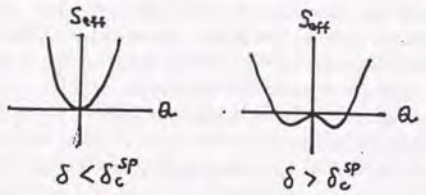

Figure 3.10: The effective action S^{eff} as a function of the pitch Q. For $\delta > \delta_c^{(sp)}$, Q has nonvanishing value and accordingly the short range spiral state is realized leading to the band motion of the hole.

which appeared because of the hole hopping. In Fig.3.9 the critical line for the short range spiral state determined by the condition of the vanishing coefficient of $O(Q^2)$ term in eq.(3.73) is plotted by a dotted line. The short range spiral state appears at lower temperature, since it is a kind of order. In the (short range) spiral state, the coherent hole hopping (i.e., band motion) is present, and so the phase is metallic.

We used the term "short range spiral" since the spiral state here does not necessarily lead to the long range magnetic order. In fact, this state is defined by $<\bar{z}_{e}z_{oi}>\sim Q$ and $<\bar{z}_{e}z_{oi}>\sim 1$. Decoupling the t-J Hamiltonian using these two expectation values, the correlation functions of the spin $\vec{S}=\bar{z}\vec{\sigma}z/2$ such as $<S^i(x)S^j(0)>$ can be calculated by a mean field approximation and seen to decay exponentially if the spins are not Bose condensed. The Bose condensation of z_σ may be prevented if the CP^1 constraint is taken into account locally, since this constraint would make the spin $z_{x\sigma}$ behave more like a fermion than a boson.

In the neutron scattering experiment[27], the spin configuration with the short range incommensurate(spiral) order is observed as a double peak in the intensity in the reciprocal space. As temperature increases, this peak is seen to change into a single peak, namely, the spiral configuration is destroyed at high temperature in accordance with our result. For instance, the sample of La-oxide with $\delta \sim 0.07$, the double peak becomes very faint at $T = 200$K.

3.8 Conclusion

We have derived an effective theory of the t-J model with weak three dimensionality at small doping assuming short range antiferromagnetic order.

At zero doping, its continuum limit is the CP^1 model as known previously. Because of very weak three-dimensionality, the Néel temperature T_N is much lower than the antiferromagnetic coupling constant $J(\simeq 1000)$K. For very small value of the anisotropy parameter α, $T_N \simeq J/(-\ln\alpha)$. We have also solved numerically the saddle point equations, and compared our results, such as the Néel temperature and the spin correlation length, to the experimental ones. The values of the parameters, J and α, that give the best fit to the data are in good agreement with the previous estimates.

Based on this effective model, the dynamics of the hole are calculated systematically. Up to one loop correction and at not very low temperature, the effect of the hole is only to decrease the effective antiferromagnetic coupling J of spins. In this case, the continuum theory is again the CP^1 model, but with parameters renormalized by the hole. Using the expression of the parameters, the Néel temperature T_N is calculated as a function of doping. With the hopping effect of the hole included, the Néel temperature decreases sufficiently fast as doping increases, consistent with experiments. The hopping effect is essential in the destruction of long range antiferromagnetic order, although only the short range hopping (shown in Fig.3.5(b)) is enough, since hopping is highly suppressed in the short range antiferromagnetic state. At very low temperature, non local interaction in the time direction can not be neglected, and as a result, the system is no longer described by the CP^1 model. The value of δ where T_N vanishes is estimated to be $\delta \sim 0.02$.

For larger doping, four and higher fermi interactions can not be neglected, and the theory is not the CP^1 again.

The advantage of our approach is that the effects of holes are taken into account rigorously, and on the resulting effective theory, the mean field approximation is done. The results on the magnetic properties are more clearly seen than the direct mean field theory on the t-J model, for instance, the effect of hole hopping on T_N can be taken into account rigorously.

We have also studied the region outside the phase with the long range antiferromagnetic order. As doping increases further after long range antiferromagnetic order is destroyed, the effective antiferromagnetic coupling $J_{\rm eff}$ finally changes sign at $\delta = \delta_c'^{p}$. For $\delta > \delta_c'^{p}$, effective ferromagnetic component of the spin interaction arises because of the hole, and accordingly, the short range spiral state is realized. The band motion of the hole appears in the (short range) spiral state. This state is used in the next section as a background spin configuration, and is shown to give rise to the superconductivity.

In our analysis, the CP^1 constraint was treated by a mean field. For the calculation of the magnetic properties, this global treatment appears good, since our results agree with experimental ones well. The local nature of this constraint will become important when the quantities like fermi surface are discussed. This point shall be mentioned in Chap.5.

Chapter 4

Superconductivity

In this chapter the superconductivity of the high T_c materials is studied on the t-J model. This chapter is based on Ref.[46]

In the previous chapter, we derived an effective lattice action eq.(3.16) in the short range antiferromagnetic spin configuration. The action contains many four and higher order fermi interactions. They were neglected at very small doping and the action was simplified to be the CP^1 action with renormalization by hole hopping. These fermi interactions, however, play the principal role in the superconductivity, and must be taken into account seriously. We can of course use this effective model also for the study of the superconductivity. However, this action contains many interaction terms arising from the integration over half of the spins. This integration in deriving the effective theory was needed to write the spin part in the form of CP^1 model, and is not necessary in the study of superconductivity. Since the essence of the superconductivity is already involved in the original t-J model, we would here rather start from the t-J model rather than the effective action derived in Chap.3. We will discuss in Sect.4.4 how the result would be modified if we perform the mean field theory of the effective action.

We again use the slave fermion representation in this chapter. In this representation, the local constraint can be treated to some extent locally by introducing the Schwinger boson (Sect.2.5). The hole fermion thereby becomes free of constraint. The essential part of the interaction between hole and spin arising from the strong correlation is therefore expected to be taken into account by this transformation. In fact, there appears in the Hamiltonian a four fermi interaction with minus sign, showing the attraction between neighboring holes. If the hole pairs are formed owing to this attraction, the superconductivity starts. To solve this four fermi theory and see this really happens, the most powerful and simple method is the mean field theory. The order parameter of the superconductivity is gauge invariant(i.e. physical) and it consists of two holes and RVB operator of spin. The calculation is carried out on the two dimensional t-J model. The applicability of the mean field theory in two-dimensions is discussed in Sect.4.4.

In our mean field theory, the spins are not treated self-consistently. We assume some configuration of spin and the spin variables are replaced by the expectation

values. As the background spin configuration, the (short range) spiral state[26] is assumed. The spiral state is obtained as a mean field solution of the slave fermion representation of the t-J model at zero temperature outside the long range antiferromagnetic phase[22]. The antiferromagnetic order of the spin is slightly broken in the short range spiral state so that the coherent hole hopping (i.e., band motion) is present. This finite hopping leads naturally to the super current once the pair is formed.

Since the order parameter on the link may exhibit non uniform pattern[23], the solution of mean field theory is searched for within the periodicity of $\sqrt{2}a$.

4.1 Mean field free energy

Let us again write the t-J Hamiltonian H_{tJ} of spins and holes in the slave fermion representation:

$$\begin{aligned} H_{tJ} &= t\sum_{x,\mu}(\psi^\dagger_{x+\mu}a^\dagger_x a_{x+\mu}\psi_x + h.c.) - \mu_c\sum_x (a^\dagger a)_x \\ &+ \frac{J}{4}\sum_{x\mu}[(a^\dagger\vec{\sigma}a)_x(a^\dagger\vec{\sigma}a)_{x+\mu} - (a^\dagger a)_x(a^\dagger a)_{x+\mu}] \end{aligned} \tag{4.1}$$

where $\psi^\dagger_x$ is the fermionic hole operator, while $a^\dagger_{x\sigma}$ is the bosonic spin operator. $\sigma(=1,2)$ is the spin index. The spin and hole operators are constrained as

$$\psi^\dagger_x\psi_x + a^\dagger_x a_x = 1 \tag{4.2}$$

for each x. (We write $a^\dagger_x a_x \equiv \sum_\sigma a^\dagger_{x\sigma}a_{x\sigma}$ etc.) The chemical potential μ_c is introduced to fix the hole concentration δ.

We rewrite H_{tJ} using the Schwinger boson $z_{x\sigma}$ defined in eq.(3.4), to see explicitly the hole-hole attraction relevant to the superconductivity. This replacement leads to the hamiltonian (3.7), which is also written as

$$\begin{aligned} H_{tJ} &= t\sum_{x,\mu}(\psi^\dagger_{x+\mu}\hat{\chi}_{x\mu}\psi_x + h.c.) + \mu_c\sum_x(\psi^\dagger\psi - 1)_x \\ &- \frac{J}{2}\sum_{x\mu}\hat{V}^\dagger_{x\mu}\hat{V}_{x\mu}\left(1 - \psi^\dagger_x\psi_x - \psi^\dagger_{x+\mu}\psi_{x+\mu} + \psi^\dagger_x\psi_x\psi^\dagger_{x+\mu}\psi_{x+\mu}\right) \end{aligned} \tag{4.3}$$

where we have used

$$|z^\dagger_x z_{x+\mu}|^2 - 1 = -\hat{V}^\dagger_{x\mu}\hat{V}_{x\mu}. \tag{4.4}$$

Here $\hat{V}_{x\mu}$ is the spin singlet (RVB) operator on the link $(x, x+\mu)$

$$\hat{V}_{x\mu} \equiv z_{x\uparrow}z_{x+\mu,\downarrow} - z_{x\downarrow}z_{x+\mu,\uparrow}, \tag{4.5}$$

and $\hat{\chi}_{x\mu}$ measures the relative orientation of the spin pair at $(x, x+\mu)$

$$\hat{\chi}_{x\mu} \equiv z^\dagger_x z_{x+\mu}. \tag{4.6}$$

The last term in the second line of eq.(4.3) is written as

$$-\frac{J}{2}\sum_{x\mu} V^{\dagger}_{x\mu}V_{x\mu}\psi^{\dagger}_{x}\psi_{x}\psi^{\dagger}_{x+\mu}\psi_{x+\mu} = -\frac{J}{2}|\psi_{x+\mu}V^{\dagger}_{x\mu}\psi_{x}|^2 \tag{4.7}$$

The minus sign here shows the attractive force between two neighboring holes arising from the antiferromagnetic interaction, as expected from the naive discussion in Sect.2.2, and as observed in the exact diagonalization[14].

We introduce accordingly an auxiliary field $\Delta_{x\mu}$ of two holes at neighboring sites wearing the cloud of singlet spin $\hat{V}_{x\mu}$:

$$\Delta_{x\mu} \equiv < \psi_{x+\mu}\hat{V}^{\dagger}_{x\mu}\psi_{x} > \tag{4.8}$$

This quantity is invariant under the U(1) gauge transformation (3.12), and thus a physical order parameter of the superconductivity carrying two units of charge. By definition it satisfies

$$\Delta_{x+\mu,-\mu} \equiv < \psi_{x}\hat{V}^{\dagger}_{x+\mu,-\mu}\psi_{x+\mu} > = \Delta_{x\mu}. \tag{4.9}$$

This order parameter represent the pair of the holes on neighboring sites. Using this auxiliary field, the four fermi term (4.7) is written by a Hubbard-Stratonovich transformation as

$$-\frac{J}{2}|\psi_{x+\mu}\hat{V}^{\dagger}_{x\mu}\psi_{x}|^2 \to -\frac{J}{2}\left(\bar{\Delta}_{x\mu}\psi_{x+\mu}V^{\dagger}_{x\mu}\psi_{x} + h.c.\right) + \frac{J}{2}|\Delta_{x\mu}|^2. \tag{4.10}$$

In our mean field theory, the spin variables $\hat{\chi}$ and $\hat{V}$ are simply replaced by some expectation values. These values are chosen as follows. In the Néel (or long range antiferromagnetically) ordered state, the expectation value of $\hat{\chi}_{x\mu} = z^{\dagger}_{x}z_{x+\mu}$ is zero, namely, the hole cannot move classically. But in the actual superconducting phase of the high T_c materials, the long range antiferromagnetic order is destroyed and only short range antiferromagnetic order remains[36]. As shown in Fig.4.1,

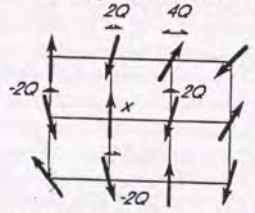

Figure 4.1: The configuration of the spiral state. The orientation of nearly antiferromagnetically ordered spins rotate by an angle of $2Q$ as x or y increase by one unit.

the deviation from the antiferromagnetic order is denoted by the small angle Q.

Choosing a suitable coordinate axis and gauge, the spin variables z at site x and $x+\mu$ are written in the form

$$z_x = \begin{pmatrix} 1 \\ 0 \end{pmatrix}, \quad z_{x\pm\mu} = \begin{pmatrix} \cos\frac{\pi\mp 2Q}{2} \\ \sin\frac{\pi\mp 2Q}{2} \end{pmatrix} \simeq \begin{pmatrix} \pm Q \\ 1 \end{pmatrix} + O(Q^2), \quad (\mu = 1,2). \tag{4.11}$$

In this incommensurate (spiral) configuration, the expectation values of the spin variables appear in eq.(4.3) are evaluated as

$$\begin{aligned} \chi_{x,\pm\mu} &\equiv < \hat{\chi}_{x,\pm\mu} > \simeq \pm Q \\ V_{x,\pm\mu} &\equiv < \hat{V}_{x,\pm\mu} > \simeq 1 \qquad (\mu = 1,2). \end{aligned} \tag{4.12}$$

As explained in Sect.3.7, this parametrization of the spin variable does not lead to long range magnetic order if the spins are not Bose condensed. The gauge we have chosen in eq.(4.11) is consistent with real fluxless $\chi_{x\mu}$ (i.e., $\prod_{\text{plaquette}} \chi_{x\mu}/|\chi_{x\mu}| = 1$). The fluxless configuration of $\chi_{x\mu}$ is energetically preferred as mentioned in some mean field theory's of spins[47].

One may, as a first assumption, take the pitch Q to be a small constant independent of δ.

$$(a) \quad Q = 0.01 \text{ and } 0.03. \tag{4.13}$$

This assumption is however, too simplified. The difference from the antiferromagnetic order must grow as doping increases. In fact, the result of the mean field analysis[22] is given by $Q \simeq (0.2 \sim 1.2) \times (t/J)\delta$ (eq.(2.11)). As a realistic ansatz, therefore, we take two values for the pitch of the spiral state.

$$(b) \quad Q = 0.17\frac{t}{J}\delta, \text{ and } 0.33\frac{t}{J}\delta. \tag{4.14}$$

In Sect.3.7, we have studied the spiral configuration at finite temperature in the mean field theory on the effective CP^1 model. Our result, however, is not applicable to low temperature region. We therefore use the results at zero temperature[22] (eq. (4.14)), assuming that this configuration persists at low temperature where the superconductivity occurs (for example, for $T \lesssim 60$K).

The state with pitch proportional to δ (eq.(4.14)) is the spiral state in the original sense (Exactly, it is called (1,1)-spiral, but in this section, we will consider only this type, and drop (1,1)- unless necessary). We will nevertheless calculate also for the simplified ansatz (4.13), to show clearly the importance of the δ-dependent pitch (or δ-dependent destruction of antiferromagnetic order). The pure spin term $-J/2\sum_{x\mu}\hat{V}^{\dagger}_{x\mu}\hat{V}_{x\mu}$ in eq.(4.3) is suppressed, since it is a constant in this treatment of spins. Also the CP^1 constraint (3.6) is not taken into account in this chapter.

Strictly speaking, we need to confirm self-consistently that the assumed spin states (4.13) (4.14) are still good spin states in the presence of the non vanishing superconducting order parameter $\Delta_{x\mu}$(The mean field theory of the spiral state[22] was done there without the superconducting order parameter). Since this has not

yet done, it is important to look into first how the superconductivity is affected by the back ground spin configurations.

From the above considerations, our mean field Hamiltonian is given by

$$\begin{aligned} H_{\rm MF} &= m\sum_x(\psi_x^\dagger\psi_x - 1) + t\sum_{x,\mu}\left(\chi_{x\mu}\psi_{x+\mu}^\dagger\psi_x + h.c.\right) \\ &- \frac{J}{2}\sum_{x,\mu}(\bar{\Delta}_{x\mu}\bar{V}_{x\mu}\psi_{x+\mu}\psi_x + h.c.) + \frac{J}{2}\sum_{x\mu}|\Delta_{x\mu}|^2. \end{aligned} \tag{4.15}$$

The expectation values χ and V are defined in eq.(4.12): The hole mass $m(=\mu_c + 2J)$ includes the renormalization by the second and the third term in the second line of eq.(4.3). In this Hamiltonian, the gauge invariance under eq.(3.12) is lost. This is unfortunately inevitable in mean field theory, where one assumes some periodicity. However, it can be shown , for instance, that another gauge choice $\chi_{x,\pm\mu} = Q, V_{x,\pm\mu} = \pm 1$ reduces by the shift in the momentum space $\vec{k} \to \vec{k} + (\pi/2, \pi/2)$ to the present choice (4.12), and thus gives the same answer.

In calculating the free energy from this Hamiltonian, we assume $\sqrt{2}a$ periodicity for $\Delta_{x\mu}$'s. Within this periodicity, independent order parameters are the four Δ_μ's ($\mu = \pm 1, \pm 2$). We divide the lattice into two sublattices (even and odd), and define the four Δ_i ($i = 1 \sim 4$) as shown in Fig.4.2. The spin expectation values

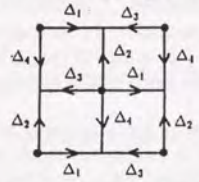

Figure 4.2: The parametrization of the four complex Δ_i's for the case of the periodicity $\sqrt{2}a$. They emerge from each odd site(marked by •) as the arrows indicate. When the periodicity is $2a$, half of the odd sites have $\Delta_i (i = 5, 6, 7, 8)$ instead of $i = 1, 2, 3, 4$. Spin variables χ_i's and V_i's are defined in the same way.

$\chi_{x\mu}$ and $V_{x\mu}$ in eq.(4.12) also have this periodicity. The four independent χ_i's and V_i's ($i = 1 \sim 4$) are defined similarly as Δ_i's, resulting in

$$\begin{aligned} \chi_i &= Q(1, 1, -1, -1) \\ V_i &= (1, 1, 1, 1). \end{aligned} \tag{4.16}$$

The Fourier transformation of the odd site hole is defined as

$$\psi_o(\boldsymbol{x}) = \frac{1}{2\pi^2}\int_\diamond d^2k\, \psi_o(k)e^{i\vec{k}\cdot\vec{x}} \tag{4.17}$$

and similarly for the even site hole ψ_e. The momentum integration $\int_\diamond d^2k$ is over the inner half of the Brillouin zone.

Using this, the partition function under the $\sqrt{2}a$ ansatz is (in the path integral representation)

$$\begin{aligned} Z &= \int D\Delta D\psi \exp\left[-\int d\tau\left[\frac{1}{2\pi^2}\int_\diamond d^2k\,\frac{1}{2}\bar{\Psi}_k M_k \Psi_k\right.\right. \\ &+ \left.\left.\sum_{x\in \rm odd}\left(\frac{J}{2}\sum_i|\Delta_i|^2 - 2\mu_c\right)\right]\right], \end{aligned} \tag{4.18}$$

where

$$\Psi_k = \left(\psi_o(k), \psi_e(k), \bar{\psi}_o(-k), \bar{\psi}_e(-k)\right)^{\rm T}, \tag{4.19}$$

and

$$M_k = \begin{bmatrix} \partial_\tau + m & t\chi_k & 0 & \frac{J}{2}\Delta_k \\ t\bar{\chi}_k & \partial_\tau + m & -\frac{J}{2}\Delta_{-k} & 0 \\ 0 & -\frac{J}{2}\bar{\Delta}_{-k} & \partial_\tau - m & -t\bar{\chi}_{-k} \\ \frac{J}{2}\bar{\Delta}_k & 0 & -t\chi_{-k} & \partial_\tau - m \end{bmatrix}. \tag{4.20}$$

The Fourier transformations of the parameters are defined as

$$\begin{aligned} \Delta_k &= V_1\Delta_1\exp(-ik_x) + V_2\Delta_2\exp(-ik_y) + V_3\Delta_3\exp(ik_x) + V_4\Delta_4\exp(ik_y), \\ \chi_k &= \chi_1\exp(-ik_x) + \chi_2\exp(-ik_y) + \chi_3\exp(ik_x) + \chi_4\exp(ik_y). \end{aligned} \tag{4.21}$$

We obtain the free energy per one site $F(\Delta_i)$ from the eigenvalues $\omega_k^{(\pm)}$ of M_k. It reads,

$$\begin{aligned} F(\Delta_i) &= -m + \frac{J}{2}\sum_{i=1}^4|\Delta_i|^2 \\ &-\frac{1}{2}\sum_\pm\int_\diamond\frac{d^2k}{2\pi^2}\left[\frac{1}{2}(\omega_k^{(\pm)} - m) + \frac{1}{\beta}\log\left(1 + \exp(-\beta\omega_k^{(\pm)})\right)\right], \end{aligned} \tag{4.22}$$

where

$$\begin{aligned} \omega_k^{(\pm)} &= \left[m^2 + |t\chi_k|^2 + \frac{J^2}{8}\left(|\Delta_k|^2 + |\Delta_{-k}|^2\right) \pm \sqrt{R}\right]^{1/2}, \\ R &= |t\chi_k|^2\left[4m^2 + \frac{J^2}{4}\left(|\Delta_k|^2 + |\Delta_{-k}|^2\right)\right] + \frac{J^4}{64}\left(|\Delta_k|^2 - |\Delta_{-k}|^2\right)^2 \\ &+\frac{t^2J^2}{4}\left(\bar{\chi}_k\bar{\Delta}_{-k}\chi_{-k}\Delta_k + c.c.\right). \end{aligned} \tag{4.23}$$

4.2 Phase diagrams

We searched for the configuration of mean field Δ_i that gives the absolute minimum of $F(\Delta_i)$ by a simulated annealing method[48]. The resulting stationally conditions are the self-consistency (gap) equations for four Δ_i's assuring $\Delta_{x\mu} = <\psi_{x+\mu}V_{x\mu}^\dagger\psi_x>$.

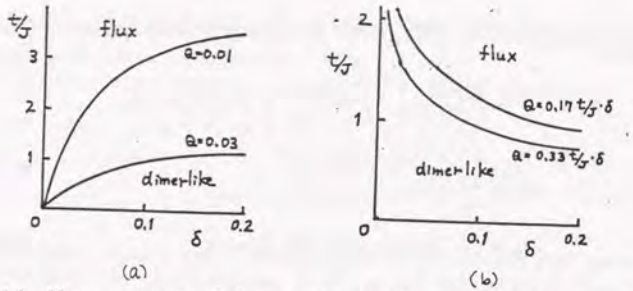

Figure 4.3: Phase structure of the ground state($T = 0$) for four ansatz for the pitch Q. (a):$Q = 0.01$, 0, 03 and (b):the spiral state: $Q = 0.17(t/J)\delta$,$0.33(t/J)\delta$.

Let us first summarize the results at zero temperature. The phase structure in $\delta - t/J$ plane at $T = 0$ for the constant pitch eq.(4.13) is shown in Fig.4.3(a). For $t = 0$, the ground state is realized in a dimer state in which only one of the four Δ_i's is nonzero (See Fig.4.4(a)). This dimer state describes the RVB state of the antiferromagnetic interactions, although there is no "resonance" since there is no hopping. The hopping term shuffles Δ_i's and so favors uniform $|\Delta_i|$'s. Thus the three Δ_i's that are zero at $t = 0$ begin to grow at $t \neq 0$ (we call it dimer-like state. See Fig.4.4(b)). The uniformity observed in the dimer and dimerlike state may develop into the phase separation[7], if the restriction on the periodicity is removed.

For sufficiently large t, the flux state supercedes the dimer-like state. This flux state is characterized by constant amplitudes $|\Delta_i| = \Delta$ and the product around each plaquette given by $\Delta_1\bar{\Delta}_2\Delta_3\bar{\Delta}_4 = -\Delta^4$, which states that the flux per plaquette is $\pm\pi$. The term flux here is defined as follows. The term $\bar{\Delta}_{x\mu}V^\dagger_{x\mu}\psi_{x+\mu}\psi_x$

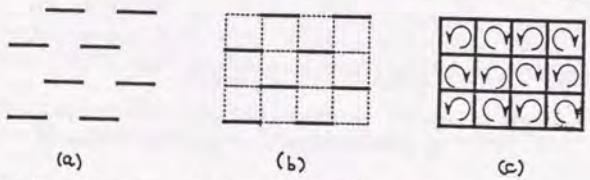

Figure 4.4: The three states, (a)dimer, (b)dimerlike and (c)flux that appear in the phase diagram Fig.4.3.

in eq.(4.15) can be regarded as a fermion hopping term if we replace $\psi_x \to \eta^\dagger_x$ for x =odd site (as in eq.(3.14)). While this fermion hops around a plaquette, this term supplies the hopping amplitude (we have set $V_i = 1$) $\Delta_2\bar{\Delta}_3\Delta_4\bar{\Delta}_1$ associated with the product $< \eta^\dagger_x\psi_{x+2}\psi^\dagger_{x+2}\eta_{x+1+2}\eta^\dagger_{x+1+2}\psi_{x+1}\psi^\dagger_{x+1}\eta_x >$ (see Fig.4.5). This amplitude is used for the definition of our flux. The flux state, with $\pm\pi$ flux, preserves the parity and time-reversal symmetry. For larger pitch $Q = 0.03$, that

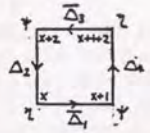

Figure 4.5: The fermion (ψ, η) get a factor of $\Delta_2\bar{\Delta}_3\Delta_4\bar{\Delta}_1$ while it hops around the plaquette $(x, x+1, x+1+2, x+2)(x \in \text{odd})$.

is, larger effective hopping, the flux state becomes more stable than for $Q = 0.01$ It is interesting to observe that every flux state we got is realized with the definite phases

$$(\Delta_1, \Delta_2, \Delta_3, \Delta_4) = \Delta(1, i, 1, i), \tag{4.24}$$

that is, the hole pairs condensate coherently. In this flux state, Δ_k of eq.(4.21) is written as $\Delta_k = \Delta(\cos k_x + i \cos k_y)$, and so it has the so called $s + id$ symmetry [20,21]. The flux state survives for any large value of t at zero temperature. In contrast, in the large-N analysis[23] in the electron hopping channel, the uniform state (corresponding to four Δ_i's being equal) is the ground state at large t/J. We note that, in the ground states obtained above, the dimer-like state and the flux state are superconducting states exhibiting the Meissner effect, while the dimer state at $t = 0$ is not (See Sect.4.4).

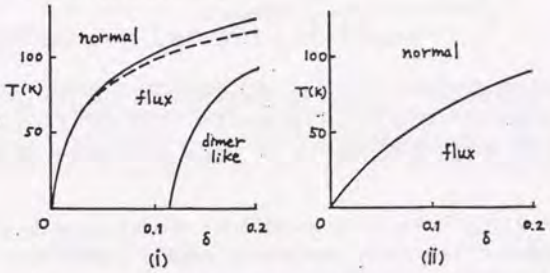

Figure 4.6: Phase diagram in $\delta - T$ plane for two pitches: (i):$Q = 0.01$ and (ii): $Q = 0.03$. For large pitch Q, the critical temperature T_c lowers, but the flux state is favored to the dimerlike state. In (i), the dashed line represents the critical temperature for the dimer state determined by Ginzburg-Landau expansion, which is lower than the T_c for the flux state.

We next consider the case of the spiral state given by eq.(4.14). The phase structure in the $\delta - (t/J)$ plane is given in Fig.4.3(b). In this case, the flux state is favored also at large value of doping, since the effective hole hopping amplitude ($t^{\text{eff}} \equiv tQ$) increases with δ. [Large $t\chi_i$ corresponds to the region of large t/J in Fig.4.3(a).]

Next, at finite temperature, one may discuss the phase structure in mean field theory. We will take $J = 0.1$eV and $t = 0.3$eV from now on. The phase diagram in $\delta - T$ plane for δ independent $Q = 0.01, 0.03$ (eq.(4.13)) is given in Fig.4.6. At high temperature is a normal(metallic) state; $\Delta_i = 0$. At T_c, there is a second order phase transition into the flux state. For the pitch $Q = 0.01$, there is a first order transition into the dimerlike state at lower temperature T_{FD}. In this dimerlike state, the values of smaller three $|\Delta_i|$'s develop as the temperature becomes higher, although four $|\Delta_i|$'s are not equal at T_{FD}. For larger pitch $Q = 0.03$, the temperature T_c lowers and also the dimerlike state disappears because of too large hopping.

Let us go on to the spiral ansatz (4.14). The phase diagram is shown in Fig.4.7. The most significant feature in this case is that the flux state at large

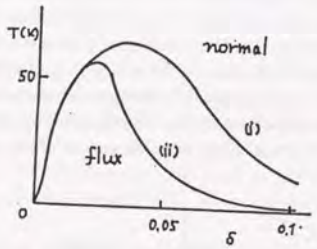

Figure 4.7: Phase diagram in $\delta - T$ plane for the spiral state with two pitches: (i):$Q = 0.17(t/J)\delta$ and (ii): $Q = 0.33(t/J)\delta$ with $t = 0.3$eV and $J = 0.1$eV. In contrast to Fig.4.6, large doping region is the normal state because of large hopping.

doping ($\delta \gtrsim (0.05 \sim 0.1)$) gives way to the normal state. this is because the effective hopping amplitude tQ becomes so large that the pairs of bounded holes are dissociated at large doping. As a result, the hole can move freely, leading to the normal state. These results show the importance of the short range antiferromagnetic order of spins (i.e., smaller pitch Q) to support the superconductivity. The dimerlike state does not appear anymore. In Fig.4.8, the temperature dependences of Δ and free energy of the flux state at $\delta = 0.017$ are plotted for the spiral state ($Q = 0.33(t/J)\delta$). The behavior of Δ looks similar to that of the conventional BCS theory.

We have also studied the case of (1,0)-spiral state[22]. This state is similar to the (1,1)-spiral state, but the pitch in, say, y-direction is zero:$\vec{Q} = (Q, 0)$. For $Q = 0.33(t/J)\delta$, it corresponds to choosing $\chi_i = \delta \times (1, 0, -1, 0)$ and $V_i \simeq 1$. Because of the anisotropic hopping, a new(line-like) configuration ($\Delta_2 = \Delta_4, \Delta_1 = \Delta_3, |\Delta_2| > |\Delta_1|$) is favored over the flux state. But the total free energy [the

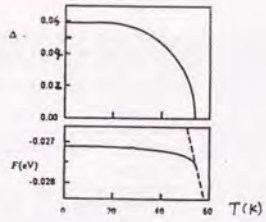

Figure 4.8: The magnitude of the order parameter Δ and the free energy of the flux state versus temperature at $\delta = 0.017$. The ansatz of the spin configuration is the spiral state with $Q = 0.33(t/J)\delta$ with $t = 0.3$eV and $J = 0.1$eV. The free energy of the normal state($\Delta_i = 0$) is plotted by a dashed line for comparison.

hole part (4.22) plus the spin part $-J/2\sum_{x\mu} V^\dagger_{x\mu} V_{x\mu}$] is higher than that for the "(1,1)-spiral + Flux" solution (say, by a few Kelvin at $\delta = 0.01$). The preference of (1,1)-spiral state to (1,0)-state in the slave fermion scheme is also observed in ref.[22] at zero temperature.

In the annealing procedure, we observed that there are several local minima. The energy difference between the flux state and other local minima is typically $\Delta F \simeq$ several Kelvin. The flux state may be stable up to fluctuations of this size.

4.3 Ginzburg-Landau expansion

A Ginzburg-Landau expansion[49] helps us to understand why the flux state is favored near the critical temperature. We here fix the gauge $\chi_i = Q(1, 1, 1, 1), V_i = (1, 1, -1, -1)$. This choice is convenient in Ginzburg-Landau expansion. The Ginzburg-Landau free energy per site up to $O(\rho^4)$ is written diagramatically as

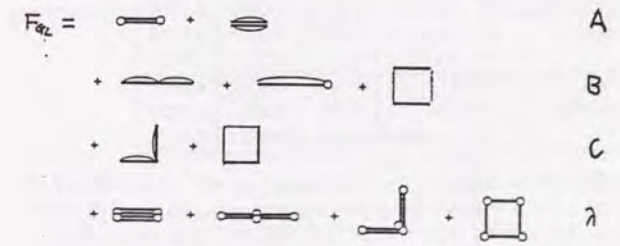

(4.25)

The order parameter Δ on link is represented by a solid line. The hole fermion propagator is denoted by dotted line:

$$\begin{aligned} \circ \quad &= \int d^2k \frac{1}{\partial_\tau + m - t\chi_k} \\ \text{—} \quad &= \int d^2k \frac{e^{ik_x}}{\partial_\tau + m - t\chi_k}. \end{aligned} \tag{4.26}$$

etc. Here the momentum integration is over the (full) first Brillouin zone (since we have not divided the lattice into sublattices), and $\chi_k = 2Q(\cos k_x + \cos k_y)$.

For the special case with the equal magnitude of four Δ_i's, $\Delta_i = \rho e^{i\phi_i}$ ($i = 1 \sim 4$), the free energy takes the form

$$\begin{aligned} F_{GL}(\rho e^{i\phi_i}) &= -4\left(A - \frac{J}{4}\right)\rho^2 - 2B\rho^2(\cos(\phi_1 - \phi_3) + \cos(\phi_2 - \phi_4)) \\ &+ C\rho^2(\cos(\phi_1 - \phi_2) - \cos(\phi_2 - \phi_3) + \cos(\phi_3 - \phi_4) - \cos(\phi_4 - \phi_1)) \\ &+ \lambda\rho^4(7 + 2\cos(\phi_1 - \phi_2 + \phi_3 - \phi_4)), \end{aligned} \tag{4.27}$$

and for the flux state $\Delta_i = \rho(1, i, 1, i)$,

$$F_{GL}(\text{flux}) = -4(A + B - \frac{J}{4})\rho^2 + 5\lambda\rho^4. \tag{4.28}$$

The coefficients A, B, C and λ are temperature dependent positive constants, and they represent terms written graphically in eq.(4.25). The critical temperature is determined by the vanishing of the term of $O(\rho^2)$, for example, by $(A + B)(T_c) - J/4 = 0$ for the flux state. The term proportional to $J\rho^2/4$ comes from $(J/2)\sum|\Delta_i|^2$ in eq.(4.15). The overall factor 4 of the term of $O(\rho^2)$ is the number of non-vanishing Δ_i's. The coefficient A represents the term in which Δ_i and $\bar{\Delta}_i$ lie on the same link, and is comparable to $J/4$, while B and C are small(see Table 4.1). The terms B, C and λ determine the relative phase of Δ_i's and accordingly

(eV)	T(K)	A	B	C	λ
$m = 0.027$(eV)	25	0.0241	0.0016	0.0001	0.1050
($\delta \sim 0.017$)	50	0.0234	0.0017	0.0007	0.0888
	75	0.0221	0.0014	0.0012	0.0681
$m = 0.037$(eV)	25	0.0180	0.0048	0.0023	0.0556
($\delta \sim 0.033$)	50	0.0173	0.0038	0.0025	0.0424
	75	0.0164	0.0030	0.0027	0.0329

Table 4.1: The coefficients of Ginzburg-Landau expansion with $Q = 0.33(t/J)\delta$ ($t = 0.3$eV, $J = 0.1$eV) for $m = 0.027$ and 0.037, corresponding to $\delta \sim 0.017$ and ~ 0.033, respectively. The critical temperature T_c is 55K and 28K, respectively.

the value of flux per plaquette. For example, one can see from eq.(4.27) that the free energy of the flux state eq.(4.28) is lower than that for the uniform state ($\Delta_i = \rho$) by $4\lambda\rho^4$. For the dimer state, the free energy is

$$F_{GL}(\text{dimer}) = -(A - \frac{J}{4})\rho^2 + \frac{1}{4}\lambda\rho^4 \tag{4.29}$$

Because of B term, which is $O(t^2)$ for small t, the critical temperature T_c for the flux state is higher than that for the dimer state (plotted by the dashed line in Fig.4.6(i)). Accordingly, the condensation starts in the flux state.

4.4 Discussion

Larger periodicity In the electron hopping channel, a new ground state other than that in the $\sqrt{2}a$-periodicity[23] was found when the periodicity is extended to $2a$[50]. Therefore, in the present approach, it is also necessary to check the stability of our flux state against larger periodicity. We have checked within the framework of Ginzburg-Landau theory that it is stable against the periodicity of $2a$. [In this case, we have eight independent Δ_i's($i = 1, ..., 8$); i.e., each odd site has four Δ_i's with either $i = 1, 2, 3, 4$ or $i = 5, 6, 7, 8$ (see the caption of Fig.4.2).] This result suggests that our flux state may survive as the true ground state of the mean field theory of the t-J model with all $\Delta_{x\mu}$'s being treated as independent mean fields. Note that the $\sqrt{2}a$-periodicity is the shortest one capable of describing the flux state.

Properties of gap In our flux state, the fermionic excitation energy reads as

$$2\omega_k = 2\left[[m - 2t\delta(\sin k_x + \sin k_y)]^2 + J^2\Delta^2(\cos^2 k_x + \cos^2 k_y)\right]^{1/2} \tag{4.30}$$

for spiral state with $Q = 0.33(t/J)\delta = \delta$. At $\delta \lesssim 0.03$, our solution gives $m - 4t\delta > 0$ (see table 4.2), owing to the large contribution from Δ. Hence ω_k is nonvanishing at any momentum, namely, the gap is S-wave like. However, at larger doping,

δ	0.017	0.033
m(eV)	0.027	0.037
T_c(eV)	0.0047	0.0024
$J\Delta(0)$(eV)	0.0060	0.0040
gap(eV)	0.0070	0.0025
2·gap/T_c	2.3	2.0

Table 4.2: The parameters at two typical value of δ at zero temperature. The pitch is $Q = \delta$. The gap is the minimum value of ω_k.

the mass is large, and accordingly the normal term $m - 2t\delta(\sin k_x + \sin k_y)$ can vanish along some fermi line $\vec{k}_F$ surrounding $\vec{k}_0 \equiv (\pi/2, \pi/2)$ (See Fig.4.9(a)). The excitation of the hole near $\vec{k}_0$ is observed also in the exact diagonalization[51] at small doping. The fermi surface is small with its area proportional to the doping δ. The gap at fermi surface $2\omega_{k_F}$ reduces to $2J\Delta_{k_F}$. The symmetry of Δ_k itself is $s + id$. Since $|\vec{k}_F - \vec{k}_0| = O(\delta^{1/2})$, excitation energy at $\vec{k}_F$ is $O(\delta^{1/2}\Delta)$ and can be regarded almost gapless in this region of δ. Our quasi-hole excitations are thus well described by the $s+id$ symmetry. The symmetry may generally depend on doping. This is not so peculiar, since the nature of the strong correlation is weakened as doping increases. The experimental results concerning to the symmetry of the order parameter seem still controversial in the present situation. For example, the temperature dependence of the penetration depth[52] is very similar to that of the BCS superconductor, which is S-wave like. On the other hand, the absence of the coherence peak below T_c in the inverse nuclear relaxation time T_1^{-1} in the NMR measurement supports the d-wave paring[53]

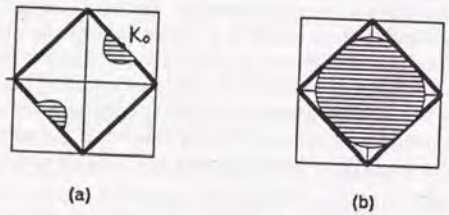

Figure 4.9: (a):The fermi surface of the hole at $\delta = 0.033$, given by $\sin k_x + \sin k_y = m/(2t\delta) = 1.8$. The shaded region is filled with holes. (b): The large fermi surface of the spin that would be obtained by exact treatment of the CP^1 constraint. See Chap.5.

The ratio 2·gap/T_c is used conventionally to determine if the system is strongly coupled or weakly coupled. The values from the photoemission experiments are obtained to be $7 \sim 8$[55]. The value of our solution is small compared even to that of the BCS theory, 3.5. Our small value, however, does not lead to the the weak coupling. Rather, the fact that Δ cannot be neglected compared to the normal term appears to indicate the system is strongly coupled.

As we have seen, in the slave fermion mean field theory, the fermi surface is small in contradiction to the photoemission study[54]. One need to go beyond the mean field theory and impose locally the CP^1 constraint $z_x^\dagger z_x = 1$ in order to obtain the large fermi surface. This may be performed by rewriting the hard core (i.e., $z_{x\sigma}^2 = 0$) boson z by a fermion and a Chern-Simons gauge field. This will be discussed in the following chapter. In the slave boson approach, on the other hand, the fermi surface is large at the mean field treatment.

Coherence length Our analysis shows that the charge carrier of the high T_c superconductor is the pair of two holes on neighboring sites. If the fluctuation of spins is taken into account, the coherence length would be about $\hbar c/J \sim 5$Å (see next chapter). According to experiments[56], the coherence length of the pair is a few times the lattice constant. In the BCS theory, the pairs are formed in the momentum space, and accordingly the coherence length is more than 10^2Å. The short coherence length in the high T_c superconductor supports the strong attractive force and the formation of the pair of holes on neighboring (or very near) sites.

Meissner effect In the presence of the electromagnetic field, the hopping term in eq.(4.3) is modified to be

$$t\psi_{x+\mu}^\dagger \hat{\chi}_{x\mu}\psi_x \to te^{ieA_{x\mu}}\psi_{x+\mu}^\dagger \hat{\chi}_{x\mu}\psi_x \tag{4.31}$$

The free energy changes to $F(\Delta_i, A)$, obtained by the replacement (4.31) in $F(\Delta_i)$ defined diagramatically in eq.(4.25). The electromagnetic current j_μ is calculated from F through $j_\mu \equiv \delta F(\Delta_i, A)/\delta A_\mu$. The term proportional to A_μ can be checked to exist, and is $O(\Delta^2)$. For no hopping $t = 0$, this current is zero. Hence the Meissner effect occurs for nonvanishing Δ and finite hopping amplitude t.

Fluctuation of Δ The mean field theory at finite temperature performed here may seem meaningless in two-dimensions owing to the infrared divergence which arise when the fluctuation around mean field is taken into account[31]. However, this is too naive.

To see this, let us include the phase fluctuation $\theta_\mu(x)$ around the order parameter so that $\Delta_{x\mu} = \Delta_\mu \exp(i\theta_\mu(x))$, where Δ_μ is the flux solution of the mean field. This mode is massless and thus possibly give rise to the infrared divergence in low dimensions. Other modes of the fluctuation are massive and does not produce divergence. Let us look into the Ginzburg-Landau free energy eq.(4.25) with the fluctuation $\theta_\mu(x)$ included:

$$\begin{aligned} F_{GL}(\theta) = &-B\rho^2 \sum_{i=1,2}\sum_{\mu=1,2} \cos\left[\theta_i(x) - \theta_i(x \pm \mu)\right] \\ &+ C\rho^2 \left[\sin(\theta_1(x) - \theta_2(x)) + \sin(\theta_2(x) - \theta_1(x + \hat{2})) \right. \\ &\left. + \sin(\theta_1(x + \hat{2}) - \theta_2(x + \hat{1})) + \sin(\theta_2(x + \hat{1}) - \theta_1(x))\right] \\ &-2\lambda\rho^4 \cos\left[\theta_1(x) - \theta_2(x) + \theta_1(x + \hat{2}) - \theta_2(x + \hat{1})\right]. \end{aligned} \tag{4.32}$$

The coefficients $(B\rho^2, C\rho^2, 2\lambda\rho^4)$ represents the terms in Fig.4.10. The values of the coefficients are obtained from the table 4.1 to be, for instance (with$Q = \delta$),

$$(B\rho^2, C\rho^2, 2\lambda\rho^4) = \begin{cases} (0.15, 0.03, 0.02) \times 10^{-5}\text{eV} & \text{for } \delta \sim 0.017, T = 55\text{K} \\ (0.19, 0.09, 0.00) \times 10^{-5}\text{eV} & \text{for } \delta \sim 0.033, T = 25\text{K}. \end{cases} \tag{4.33}$$

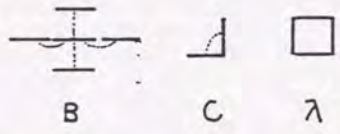

Figure 4.10: The couplings of the phase fluctuation around the flux state

The dominant term $B\rho^2$ represents the ferromagnetic coupling between two XY spins $\theta_i(x)$ and $\theta_i(x \pm \mu)$ on the nearest neighbor links. This term does not contain the interaction between two spins $\theta_1(x)$ and $\theta_2(y)$. Therefore, the phase fluctuation around the flux state at $\delta \sim 0.02$ is well described by the (two sets $\mu = 1, 2$ of) ferromagnetic XY model $\theta_\mu(x)$, with the coupling constant $B\rho^2$ dependent on the mean field magnitude ρ.

The XY model in two-dimensions has Kosterlitz-Thouless transition at $T_{\rm KT}$. Below this $T_{\rm KT}$, the system is superconducting although there is no long range order. In fact, the coupling of the XY variable $\theta(x)$ to the electromagnetic field $A_\mu(x)$ is written as

$$|(\partial_\mu - ieA_\mu)\Delta e^{i\theta(x)}|^2 = |(\partial_\mu\theta - eA_\mu)\Delta|^2. \tag{4.34}$$

This term give rise to the mass term $e^2\Delta^2 A_\mu^2$ of the gauge field, and thus the Meissner effect occurs (Anderson-Higgs mechanism). This Kosterlitz-Thouless transition would change into a second order transition when weak three dimensionality is added. This scenario is checked in another model; the continuum four fermi theory with chiral U(1) symmetry[57]. The resulting transition point T_c' is the true critical temperature of the real high T_c superconductor. This temperature T_c' becomes higher as three-dimensionality increases[40], just as the Néel temperature T_N does (Fig.3.7).

The C-term in eq.(4.32) grows for larger doping, and the two XY spins $\theta_1(x)$'s and $\theta_2(x)$'s are no longer decoupled for, say, $\delta \gtrsim 0.03$ for $Q = \delta$. The term λ in eq.(4.32) is invariant under the local U(1) gauge transformation (Do not confuse this with the U(1) gauge transformation of hole and spin (3.12).)

$$\theta_\mu(x) \to \theta_\mu(x) + \eta(x+\mu) - \eta(x). \tag{4.35}$$

The terms B and C breaks this invariance. Therefore, if B and $C$are small compared to λ, the mode (4.35) of the phase fluctuation are not suppressed, and accordingly, the expectation value of $\Delta_{x\mu}$ vanishes: $< \Delta_{x\mu} > \propto < \exp(i\theta_\mu(x)) > = 0$. This may happen at small region of delta, since λ increases and B and C decrease for smaller doping. If this really happens, the superconductivity would start at $T = 0$ from finite δ just as experimentally observed, not from $\delta = 0$ as in Fig.4.7.

It is expected that the three-dimensional mean field theory would give similar result as that of ours in two-dimensions. This is confirmed to some extent[58]. Accordingly, our study may have meanings also in this sense.

Fluctuation of spin We have done calculation with the the background of classical spins. Next question is, how the result is modified by the fluctuation of the spin?

Some of the effects of spin fluctuation can be seen from the effective lattice action (3.16) obtained by integrating out half of the spins. In fact, this action contains three terms of four fermi interaction. These terms come from the second, third terms and T_{4f}', and relevant terms are (with ψ_o recovered from $\eta = U\bar{\psi}_o$, and with $\alpha = 0$),

$$\begin{aligned} T_{4f} = \int d\tau \sum_o \Big[& -\frac{J}{2}\sum_i \bar{\psi}_o\psi_o\bar{\psi}_{oi}\psi_{oi}(\bar{z}_{oi}z)(\bar{z}z_{oi}) \\ & -\frac{J}{2}\int d\tau \sum_o \sum_{ij} \bar{\psi}_i\bar{\psi}_j\psi_j\psi_i(\bar{z}_i z)(\bar{z}z_j)(\bar{z}_j\bar{z})(\bar{z}z_i) \\ & -\frac{t^2}{2J}\sum_{i,j}\eta_o\psi_{oi}\bar{\psi}_{oj}\bar{\eta}_o(\bar{z}_{oi}z_e)(\bar{z}_e z_{oj})\Big]. \end{aligned} \tag{4.36}$$

The first term is classical term, and is essentially the same as that we have obtained in the original t-J model (eq.(4.7)), since $(\bar{z}_{oi}z) \simeq V_{x\mu} \simeq 1$ in the short range antiferromagnetic order. New terms arising from the spin fluctuation are the second and the third terms in (4.36). The second term is the attractive force between two holes on next nearest neighbor site (Fig.4.11(a)). Although its strength$\simeq J < \bar{z}z_{oi} >< \bar{z}_{oj}z >$ is small in the short range antiferromagnetic order. The third term is written as

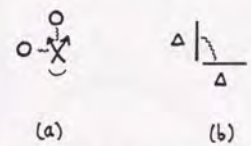

Figure 4.11: The effects of spin fluctuation on superconductivity. (a):To cause attractive force between next nearest neighbor holes. (b):To fix the relative phase of the neighboring order parameters $\Delta_{x\mu}$.

$$\sim \frac{t^2}{2J}|\sum_i \Delta_{oi}|^2, \tag{4.37}$$

and is important to determine the relative phase of neighboring $\Delta_{x\mu}$'s (Fig.4.11(b)).

It can be checked by integrating out the rest of the spins that the further fluctuation give rise through J-term to the attractive force between two holes at a distance. This force becomes exponentially small at large distance in the absence of long range antiferromagnetic order. Its range would be typically $hc/J \sim 0.5(\text{eV\AA})/0.1(\text{eV}) \sim 5\text{\AA}$. As a result, pairs Δ_{xy} of holes at x and y with $|x-y| \lesssim$ (a

prevent these terms to cause the phase separation. It is, however, difficult to show this explicitly.

One of the possible way to see the effect of spin fluctuation on superconductivity is to carry out the mean field theory with both $\Delta_{x\mu}$ and the order parameter of spins $\chi_{x\mu}$ and $V_{x\mu}$ included in the mean field equations.

Chapter 5

Summary and Discussions

Summary We have seen that the t-J model describes well the global properties of high T_c materials in both antiferromagnetic and superconducting phase. The phase diagram obtained is shown in Fig.5.1. Explanation of the phase diagram

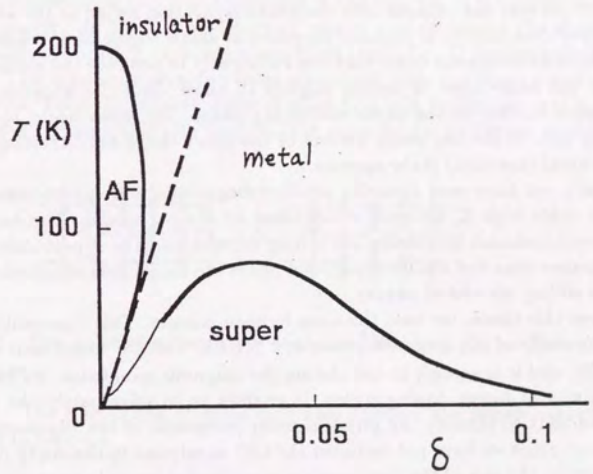

Figure 5.1: The phase diagram of the high T_c material calculated from the t-J model.

based on our analysis goes as follows.

The strong antiferromagnetic spin interaction ($J \simeq 1000$K) produces at small doping and low temperature the long range antiferromagnetic (Néel) order. Because of the quasi two-dimensionality, the transition temperature T_N is lower than J by a factor $|\ln \alpha|^{-1} \sim 1/5$. The effective antiferromagnetic coupling $J_{\rm eff}$ dimin-

ishes by the hole doping, and consequently the Néel temperature T_N decreases as doping increases. The hopping effect of the hole in particular is important in the destruction of antiferromagnetic order. However, only short range hopping dominates, since the hopping is highly suppressed in the antiferromagnetic phase. Outside the antiferromagnetic phase, spins are still in the firm short range antiferromagnetic order, although the magnetization vanishes. This short range antiferromagnetic order develops at low temperature into the short range spiral state, where the spins rotate spatially with some finite pitch. In this state, the band motion of the hole is present. The (short range)antiferromagnetic order produces an attractive force between neighboring holes owing to the antiferromagnetic interaction J. As a result, the hole pairs are formed at low temperature and the superconductivity starts. The origin of the *high* critical temperature is the large value of the spin antiferromagnetic coupling J, being much stronger than the phonon coupling in BCS theory. The coherence length is very small ($\sim$ a few lattices) because of the strong pairing force. The absence of long range antiferromagnetic order is needed in the superconductivity, since finite amplitude of hole hopping is necessary to produce the superconducting current. Finite hopping is also needed to prevent the collapse into the phase separation owing to the attraction. The superconductivity is possible therefore at small region of δ, where the short range antiferromagnetic order survives sufficiently to produce the attractive force, and at the same time, is broken slightly to allow the finite hopping. As doping increases further in the superconducting phase, the holes begin to flow independently due to the too much decline of the short range antiferromagnetic order, and normal (metallic) state appears.

In summary, we have seen that the antiferromagnetism and superconductivity of the Cu oxide high T_c material is described by the t-J model. The essence lies in the local constraint expressing the strong correlation. The superconductivity, its appearance near the antiferromagnetic phase are explained consistently by including the strong correlated nature.

Throughout this thesis, we used the slave fermion scheme. This representation is good for the study of the magnetic phase at $\delta \lesssim 0.05$. The CP^1 constraint is included globally, and it is enough in calculating the magnetic quantities. As for the superconductivity at larger doping region, it enables us to solve partly the local constraint and thus to identify the physical order parameter of the superconductivity. However, since we have not included the CP^1 constraint in the study of the superconductivity, the size of the fermi surface is contradictory to the experiments in the region of moderate doping ($\delta \gtrsim 0.1$). To remedy this point, the mean field treatment of the constraint would not be enough, too, and the local treatment of the CP^1 constraint would be needed. This is one of the important remaining problem in the slave fermion scheme (see below).

Possible improvements Our analysis reproduced well the global properties of the high T_c material. There are, however, several flaws in our phase diagram. First, our antiferromagnetic-normal phase boundary ends at $\delta = 0$ at zero temperature.

The two loop correction by holes, localized in the same way, shifts this T_N-δ line to larger δ region, but (together with higher loops) is not enough to stop the reentrant behavior. This behavior is owing to the high temperature expansion of the correction by the hole hopping. To improve this point, the renormalization group method[30,59] on the effective action of the hole and spin (3.16) may be useful. In fact, no pathological behavior would appear at low energy on integrating out the fast (i.e., high momentum) component of the fields.

Secondly, our superconducting phase starts at $T = 0$ from $\delta = 0$. This would be improved if the T_N-δ line reaches finite δ at $T = 0$, since the superconductivity cannot occur in the long range antiferromagnetic order because of no hopping. It may be also possible, as discussed in Sect.4.4, the fluctuation around $\Delta_{x\mu}$ remedies it. Anyway, in this region near the border of the antiferromagnetic and the superconducting phase at low temperature, both spins $z_{x\sigma}$ and holes ψ_x play important roles and thus the rigorous calculation on the effective action (3.16) is not possible. A new approach may be needed.

Thirdly, the superconductivity ends in our solution too fast in our calculation, at $\delta \sim 0.1$. These are expected to be due to the mean field treatment of spins. In fact, the spiral solution $Q \propto \delta$ was obtained in the absence of the superconducting order parameter. In the superconducting phase, the decline of the short range antiferromagnetic order is expected not to be so rapid, i.e., Q develops more slowly then $\propto \delta$. This is because once two holes are paired, they can move about without disturbing the antiferromagnetic order of spins (Fig.5.2), unlike the case of a single hole (Fig.3.4). Taking this into account, the superconducting state would extend

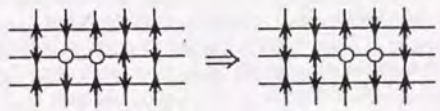

Figure 5.2: The hole pairs can move without disturbing the antiferromagnetic order of spins.

to large δ. The fluctuation of spins may also enhance the superconductivity as mentioned in Sect.4.4.

Fermi surface We have studied the t-J model in the slave fermion representation. In this approach, the fermionic degree of freedom is the hole only, and accordingly the fermi surface is small with area proportional to doping (Fig.4.9(a)) in the mean field approximation. The small fermi surface is observed in the exact diagonalization[51] at small doping ($\delta = 1/20$), and also, the doping dependence of the Hall coefficient ($\propto 1/\delta$) is understood easily assuming the small fermi surface for the charge degrees of freedom[60]. At larger doping ($\delta \gtrsim 0.1$), on the other hand, large fermi surface is observed in the exact diagonalization[61]. In

the angle-resolved photoemission experiments[54], the existence of large fermi surface of electrons is confirmed. Our small fermi surface (of holes) may accordingly appear inconsistent with experiments. However, this is not necessarily true.

The Schwinger boson z is constrained by $\sum_\sigma z^\dagger_{x\sigma} z_{x\sigma} = 1$. This CP^1 constraint, after the attractive force between holes is taken away, appears unimportant. However, this has still an important role: to the let the spin excitations behave fermionic, and accordingly to produce large fermi surface. In fact, owing to the CP^1 constraint, the allowed states of each site are the following three:

$$|nm> = |00>, \quad |10>, \quad |01>, \tag{5.1}$$

where n and m are the number of $z_\uparrow$ and $z_\downarrow$ particle, respectively. If this constraint is treated only globally, on the other hand, all the states with larger particle numbers $n, m = 0 \sim \infty$ are included. Thus, in the mean field treatment of the constraint, these bosons with hard core nature (i.e. $z^2_{x\uparrow} = z^2_{x\downarrow} = 0$ (from (5.1))) are described much better by fermions than by bosons, as the severe restriction (5.1) indicates. Let us therefore replace these hard core bosons $z_{x\sigma}$ by fermions $f_{x\sigma}$ to get the rough idea of large fermi surface. [Exactly speaking, the hard core bosons are mapped using the Jordan-Wigner transformation to the system of fermions and Chern-Simons gauge field in two-dimensions[62]. Simple replacement $z_{x\sigma} \to f_{x\sigma}$ is equivalent to neglecting the Chern-Simons field. This replacement is exact in one dimension, where no Chern-Simons gauge field is needed in the transformation.] The resulting Hamiltonian of the fermionic spin (dropping the contributions of the holes) is essentially that of the slave boson t-J model. mean field theories[21,47] indicate that the order parameter of fermionic spin singlet pair has d-wave symmetry. Consequently, the spin fermions with density $(1-\delta)$ fill the shaded region in Fig.4.9(b). The fermi surface of spins is large (area$\propto (1-\delta)$), consistent with experiments. More precisely, only the (physical) electron can be observed in experiments such as the photoemission. The electron is written as a product of the hole and spin, $c_{x\sigma} = \psi^\dagger_x a_{x\sigma}$, and accordingly, if both the hole and spin truly behave like fermions because of the constraint, the fermi surface of the electron would be the combination of those of the hole- and spin-"fermion". Therefore, the small fermi surface of the hole may not be inconsistent with experimentally observed large fermi surface, because of the dynamics of the spin.

Is two-dimensionality essential? In our arguments based on mean field theory and on the analogy with XY model, the stronger the three-dimensionality becomes, the higher the critical temperature T_c is. This is consistent with the experimental results that the T_c rises as the pressure increases[63], since the three-dimensionality is expected to increase at high pressure. Also, the experiments on the superlattice[64] show that the critical temperature decreases rapidly as the distance between CuO layers increases.

Then what about the fact that the high T_c materials have all quasi two-dimensional structure, and that the three-dimensional Cu oxides do not show superconductivity[65]? One possibility is that, with full three-dimensionality, the

antiferromagnetic phase becomes so dominant that the superconducting phase can not appear. In fact, the Néel temperature is very high ($O(J) \simeq 1000$K) near the full three-dimensionality (see Fig.3.7). The antiferromagnetic phase would accordingly expand to the larger doping region, swallowing up the region suitable for would be the superconductivity. It may be said that the antiferromagnetic order, being a direct result of the antiferromagnetic spin interaction, is stronger than the superconductivity, which arises from the balance among the antiferromagnetic spin interaction, hole density and mobility of holes.

Gauge theory approach We have solved the local constraint of the t-J model by introducing the Schwinger boson through eq.(2.12). This makes the attractive force between holes seen explicitly in the Hamiltonian. If one does not use this technique, and treat the constraint by global mean field, one must take into account the fluctuation around the mean field of the lagrange multiplier λ dynamically in order to include the strongly correlated nature. In this case, the scenario of superconductivity according to Ref.[66] would go like this. The fluctuation behaves as the time component of the U(1) gauge field. This gauge field works as attractive for hole fermions on different sublattices, and consequently the neighboring holes would form a pair.

Normal state We have not referred to the normal state phase. The high T_c material in this phase is an usual metal but its behaviors are not so *normal* compared to conventional metals. For instance, the resistivity at low temperature (but, of course, for $T > T_c$) is proportional to the temperature[67]. In the normal metal, where the resistivity is dominated by the scattering by phonons, it diminishes at low temperature much rapidly than $\propto T$. It is also observed that the Hall coefficient R_H of the superconductor $YBa_2Cu_3O_{7-\delta}$ depends on the temperature: $R_H \propto 1/T$[68], in contrast to its T-independence in the usual metal. This behavior of R_H, however, varies from the material. For example, R_H does not depend on T in the La-superconductor[4]. Another peculiarity is observed in the behavior of the nuclear relaxation time T_1 of the Cu atom[69]: T_1 does not satisfy the Korringa law $T_1^{-1} \propto T$ of the conventional metal. These unusual behaviors are due to the nature of the strong correlation. The local constraint of the t-J model plays an important role still in the metallic phase. In fact, because of this constraint, some non fermi liquid behavior may appear just as in the case of the one dimensional t-J model, and the above peculiarities might be explained. Actually, a phenomenological model of a non fermi liquid (called the marginal liquid) reproduces the above abnormal properties of the normal state[70], although its microscopic justification does not yet exist. In Ref.[71], the abnormal behaviors are explained by including the spin fluctuation (they call it the gauge field) around the mean field up to one loop. This supports the importance of the constraint in the normal state.

Acknowledgement

I am grateful to I. Ichinose, T. Matsui and H. Yamamoto for collaboration. I would like to thank Professor T. Terasawa and his colleagues at university of Tokyo, Komaba. I also thank C. Itoi, N. Kawakami T. Minoguchi and K. Sakakibara for comments.

Bibliography

[1] J.G.Bednorz and K.A.Müller, Z.Phys. **B64**, 189 (1986).

[2] S. S. Parkin, V. Y. Lee, E. M. Engler, A. I. Nazzal, T. C. Huang, G. Gorman, R. Savoy and R. Beyers, Phys. Rev. Lett. **60**, 2539 (1988).

[3] H. Yoshida, Parity **3** (1988).

[4] S. Uchida, H. Takagi, H. Ishii, H. Eisaki, T. Yabe, S. Tajima and S. Tanaka, Jpn. J. Appl. Phys. **26**, L440 (1987).

[5] M. Imada and Y. Hatsugai, J. Phys. Soc. Jpn. **58**, 3752 (1989); J. Bonca, P. Prelovsek and I. Sega, Phys. Rev. **B39**, 7074 (1989).

[6] C. E. Gough, M. S. Colclogh, E. M. Forgan, R. G. Jordan, M. Keene, C. M. Muirhead, A. I. M. Rae, N. Thomas, J. S. Abell and S. Sutton, Nature **326**, 855 (1987); J. S. Tsai, Y. Kubo and J. Tabuchi, Phys. Rev. Lett. **58**, 1979 (1987).

[7] V.J.Emery,S.A.Kivelson and H.Q.Lin, Phys. Rev. Lett. **64** 475 (1990).

[8] M. Ogata, M. Luchini, S. Sorella and F. F. Assad, preprint.

[9] P. W. Anderson, Science **235**, 1196 (1987);

[10] Y-H. Chen, F. Wilczek, E. Witten and B. I. Halperin, Int. J. Mod. Phys, **B3**, 1001 (1989); K. Kitazawa, H. Murayama, Nucl. Phys. **B338**, 777 (1990); Y. Hosotani and S. Chakravarty, Phys. Rev. **B42**, 342 (1990).

[11] R. F. Kiefl, J. H. Brewer, I. Affleck, J. F. Carolan, W. N. Hardy, T. Hsu, R. Kadono, J. R. Kempton, S. R. Kreitzman, Q. Li, A. H. O'Reilly, T. M. Riseman, P. Schleger, P. C. E. Stamp, H. Zhou, L. P. Le, G. M. Luke, B. Sternlieb, Y. J. Uemura, H. R. Hart and K. W. Lay, Phys. Rev. Lett. **64**, 2082 (1990);
S. Spielman, K. Fesler, C. B. Eom, T. H. Geballe, M. M. Fejer and A. Kapiturnik, Phys. Rev. Lett. **65**. 123 (1990).

[12] A. Fujimori, S. Takekawa, E. Takayama-Muromachi, Y. Uchida, A. Ono, T. Takahashi, Y. Okabe, and H. Katayama-Yoshida, Phys. Rev. **B39**, 2255 (1989).

[13] F. C. Zhang and T. M. Rice, Phys. Rev. **B37**, 3759 (1988).

[14] M. Imada, J. Phys. Soc. Jpn, **57**, 3128 (1988); J. E. Hirsch and H. Q. Lin, Phys. Rev. **B37**, 5070 (1988).

[15] J. E. Hirsch, Phys. Rev. Lett. **54** (1985) 1317.

[16] Z. Zou and P. W. Anderson, Phys. Rev. **B37**, 627 (1988).

[17] M. C. Guzwiller, Phys. Rev. Lett. **10**, 159 (1963); Phys. Rev. **134**, A293 (1964);**137**, A1726 (1965).

[18] C. Gros, R. Joynt and T. M. Rice, Phys. Rev. **B36**, 381 (1987).

[19] G. Baskaran, Z. Zou and P.W. Anderson, Solid State Comm. **63**, 973 (1987).

[20] G. Kotliar, Phys. Rev. **B37**, 3664 (1988).

[21] G. Kotliar and J. Liu, Phys. Rev. **B38**, 5142 (1988);
Y. Suzumura, Y. Hasegawa and H. Fukuyama, J. Phys. Soc. Japan **57**, 2768 (1988).

[22] D. Yoshioka, J. Phys. Soc. Japan **58**, 1516 (1988); C. Jayaprakash, H. R. Krishnamurphy and S. Sarker, Phys. Rev. B40, (1989) 2610; C. L. Kane, P. A. Lee, T. K. Ng, B. Chakraborty and N. Read, Phys. Rev. B41, (1990) 2653; B. Chakraborty, N. Read, C. Kane and P. A. Lee, Phys. Rev. B42, (1990) 4819.

[23] I. Affleck and J. B. Marston, Phys. Rev. **B37**, 3774 (1988); J. B. Marston and I. Affleck, Phys. Rev. **B39**, 11538 (1989).

[24] E. Manousakis and R. Salvador, Phys. Rev. Lett. **60** (1988), 840.

[25] D. P. Arovas and A. Auerbach, Phys. Rev. **B38**, 316, 1988; D. Yoshioka, J. Phys. Soc. Japan **58**, 32 (1988).

[26] B. Schraiman and E. Siggia, Phys. Rev. Lett. **62**, 1564 (1989).

[27] T. R. Thurston, R. J. Birgeneau, M. A. Kastner, N. W. Preyer, G. Shirane, Y. Fujii, K. Yamada, Y. Endoh, K. Kakurai, M. Matsuda, Y. Hidaka and T. Murakami, Phys. Rev. **B40**, 4585 (1989).

[28] S-W. Cheong, G. Aeppli, T. E. Mason, H. Mook, S. M. Hayden, P. C. Canfield, Z. Fisk, K. N. Clausen and J. L. Martinez, Phys. Rev. Lett **67**, 1971 (1991).

[29] F. D. Haldane, Phys. Lett. **A93**, 464 (1983); Phys. Rev. Lett. **50**, 1153 (1983).

[30] S. Chakravarty, B. I. Halperin and D. R. Nelson, Phys. Rev. Lett. **60** (1988) 1057; Phys. Rev. **B39** (1989) 2344.

[31] N. D. Mermin and H. Wagner, Phys. Rev. Lett. **17**, 1133 (1966); P. C. Hohenberg, Phys. Rev. **158**, 383 (1967).

[32] P. Schlottmann, Phys. Rev. **B36**. 5177 (1987).

[33] F. D. M. Haldane, Phys. Rev. Lett. **45**, 1358 (1980); **47**, 1840 (1981); J. Phys. **C14**, 2585 (1981); Phys. Lett. **81A**, 153 (1981).

[34] I. Ichinose and T. Matsui, Mod. Phys. Lett. **B4**, 995 (1990); Phys. Rev.**B** to appear.

[35] H. Yamamoto, G. Tatara, I. Ichinose and T. Matusi, Phys. Rev. **B44**, 7654 (1991).

[36] Y. Endoh, K. Yamada, R. J. Birgeneau, D. R. Gabbe, H. P. Jensen, M. a. Kastner, C. J. Peters, P. J. Picone, T. R. Thurston, J. M. Tranquada, G. Shirane, Y. Hidaka, M. Oda, Y. Enomoto, M. Suzuki, and T. Murakami, Phys. Rev. B **37**, 7443 (1988).

[37] A. DÁdda, P. Divecchia and M. Lüscher, Nucl. Phys. B146, 63 (1978); B152, 125 (1979); E. Witten, Nucl. Phys. B149, 285 (1979).

[38] I. Ya. Areféva and S. I. Azakov, Nucl. Phys. B162 (1980) 298.

[39] I. Ichinose and H. Yamamoto, Mod. Phys. Lett. **A5**, 1373 (1990).

[40] S. Hikami and T. Tsuneto, Prog. Theor. Phys. **63**(1980), 387

[41] W. Janke and T. Matsui, Phys. Rev. **B42**, 10673 (1990).

[42] B. Rosenstein, B. J. Warr and S. H. Park, Nucl. Phys. B336, 435 (1990).

[43] E. Brézin and J. Zinn-Justin, Phys. Rev. **B14**, 3110 (1976).

[44] K. B. Lyons, P. A. Fleury, J. P. Remeika, A. S. Cooper and T. J. Negran, Phys. Rev. **B37**, 2353 (1988).

[45] T. Thio, T. R. Thurston, N. W. Preyer, M. A. Kastner, H. P. Jenssen, D. R. Gabbe, C.Y. Chen, R. J. Birgeneau, and A. Aharony, Phys. Rev. **B38**,905 (1988).

[46] G. Tatara and T. Matsui, Phys. Rev. **B44**, 2867 (1991).

[47] F. C. Zhang, Phys. Rev. Lett. **64**, 974 (1990).

[48] S. Kirkpatrick, C. D. Gelatt, Jr. and M. P. Vecchi, Science **220**, 671(1983).

[49] G. Baskaran and P. W. Anderson, Phys. Rev. **B37**, 580 (1988); A. Nakamura and T. Matsui, Phys. Rev. **B37**, 7940 (1988); T. Matsui, Int. J. Mod. Phys. **B1**, 613 (1988).

[50] T. Dombre and G. Kotliar, Phys. Rev. **B39**, 855 (1989).

[51] T. Itoh, M. Arai and T. Fujiwara, Phys. Rev. **B42**, 4834 (1990).

[52] L. Krusin-Elbaum, R. L. Greene, F. Holtzberg, A. P. Malozemoff and Y. Yeshurun, Phys. Rev. Lett. **62**, 217 (1989).

[53] P. C. Hammel, M. Takigawa, R. H. Heffner, Z. Fisk and K. C. Ott, Phys. Rev. Lett. **63**, 1992 (1989).

[54] T. Takahashi, H. Matsuyama, H. Katayama-Yoshida, Y. Okabe, S. Hosoya, K. Seki, H. Fujimoto, M. Sato and H. Inokuchi, Phys. Rev. **B39**, 6636 (1989); G. Mante, R. Claessen, T. Buslaps, S. Harm, R. Manzke, M. Skibowski and J. Fink, Z. Phys.**B80**, 181 (1990); C. G. Olson, R. Liu, A. -B. Yang, D. W. Lynch, A. J. Arko, R. S. List, B. W. Veal, Y. C. Chang, P. -Z. Jiang and A. P. Paulikas, Sience **245**, 731 (1989).

[55] H. Takagi, T. Ido, S. Ishibashi, M. Uota, S. Uchida and Y. Tokura, Phys. Rev. **B40**, 2254 (1989); J. M. Imer, F. Patthey, B. Darbel, W-D. Schneider, Y. Baer, Y. Petroff and A. Zettle, Phys. Rev. Lett. **62**, 336 (1989); C. G. Olson, R. Liu, A. B. Yang, D. W. Lynch, A. J. Arko, R. S. List, B. W. Veal, Y. C. Chang, P. Z. Jiang and A. P. Paulikas, Science **245**, 731 (1989).

[56] Y. Iye, T. Tamegai, T. Sakakibara, T. Goto, N. Miura, H. Takeya and T. Takei, Physica **C153-155**, 26 (1988); U. Welp, W. K. Kwok, G. W. Crabtree, K. G. Vandervoort and J. Z. Liv, Phys. Rev. Lett. **62**, 1908 (1989); D. E. Farrel, C. M. Williams, S. A. Wolf, N. B. Bansal and V. G. Kogan, Phys. Rev. Lett. **63**, 782 (1989).

[57] H. Yamamoto and I. Ichinose, to appear in Nucl. Phys. **B**.

[58] K. Sakakibara, I. Ichinose and T. Matsui, preprint (1991).

[59] T. Yamagisawa, preprint.

[60] H. Fukuyama Y. Hasegawa, Physica **148B**, 204 (1987).

[61] P. Horsch and W. Stephan, Physica **C185-189**, 1585 (1991).

[62] E. Fradkin, Phys. Rev. Lett. **63**, 322 (1989).

[63] C. Murayama, N. Mori, S. Yomo, H. Takagi, S. Uchida and Y. Tokuma, Nature **339**, 293 (1989).

[64] Q. Li et al., Phys. Rev. Lett. **64**, 3086 (1990); D. H. Lowndes et al., Phys. Rev. Lett. **65**, 1160 (1990).

[65] T. Tamegai and Y. Iye, Physica **C159**, 181 (1989).

[66] P. B. Wiegmann, Phys. Rev. Lett. **60**, 821 (1988).

[67] M. Gurvitch and A. T. Fiory, Phys. Rev. Lett. **59**, 1337 (1987).

[68] A. P. Ong, Z. Z. Wang, J. Clayhold, J. M. Tarascon, L. H. Greene and W. R. McKinnon, Phys. Rev. **B35**, 8807 (1987).

[69] K. Ishida, Y. Kitaoka and K. Asayama, J. Phys. Soc. Jpn **58**, 36 (1989); T. Imai, H. Yasuoka, T. Shimizu, Y. Ueda and K. Kosuge, J. Phys. Soc. Jpn **58**, 1528 (1989).

[70] C. M. Varma, P. B. Littlewood, S. Schmitt-Rink, E. Abrahams and A. Ruckenstein, Phys. Rev. Lett. **63**, 1996 (1989).

[71] N. Nagaosa and P. A. Lee, Phys. Rev. Lett. **64**, 2450 (1990).